Westinghouse ENGINEER March 1969

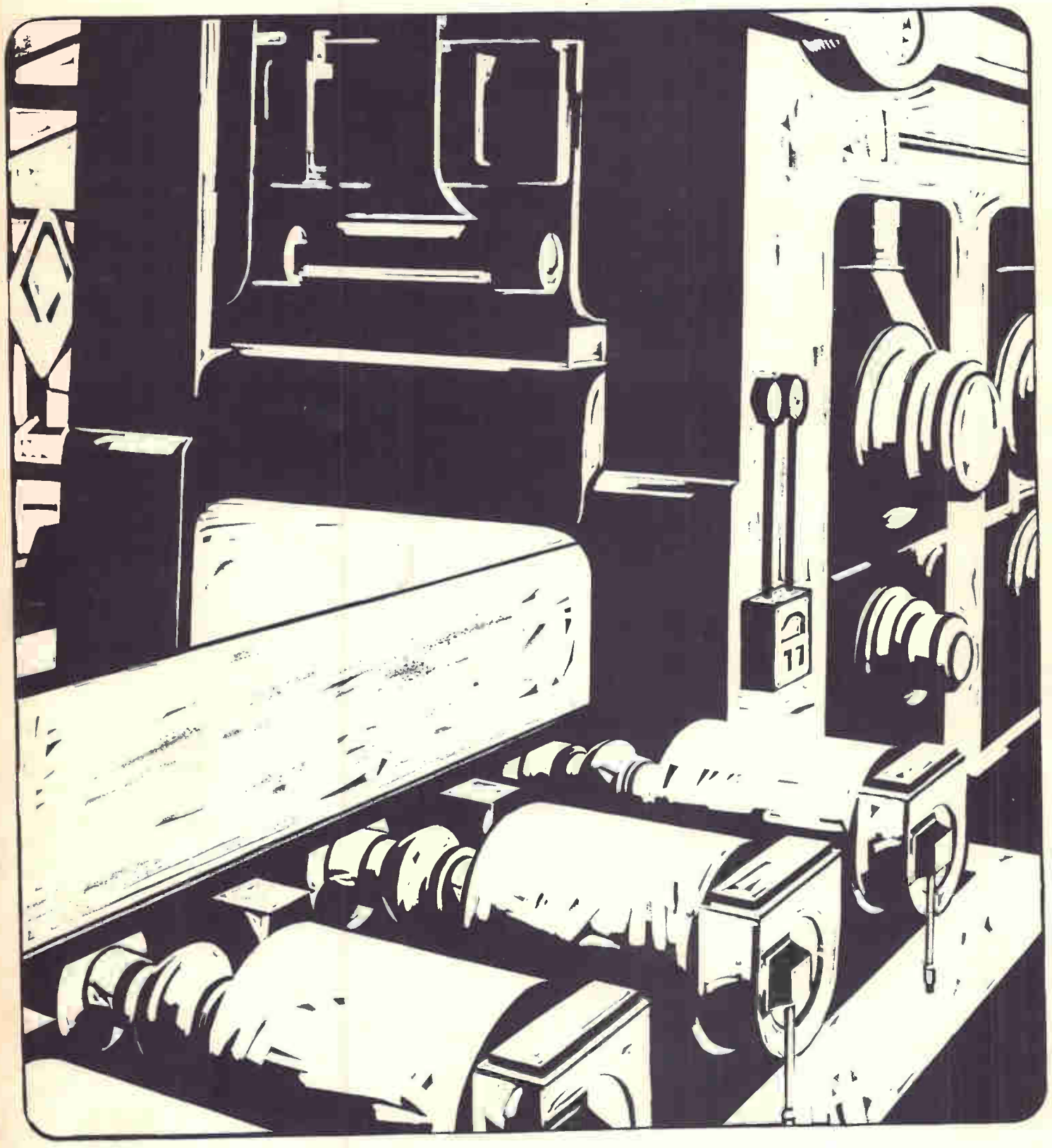

The top picture, clearly showing the large galaxy NGC-6946, was made in two seconds with a telescope and low-light-level television equipment. The bottom picture of the same area of sky was made by the conventional procedure of exposing a photographic plate directly through the telescope; it barely shows the same galaxy after an exposure of an hour and a half. Both pictures were made with the 36-inch telescope at the McDonald Observatory of the University of Texas. The television equipment, consisting of an electrostatic image intensifier coupled to an SEC camera, is being developed by Westinghouse engineers to speed surveys of the heavens. Another application of SEC image tubes in astronomy is described on page 63.

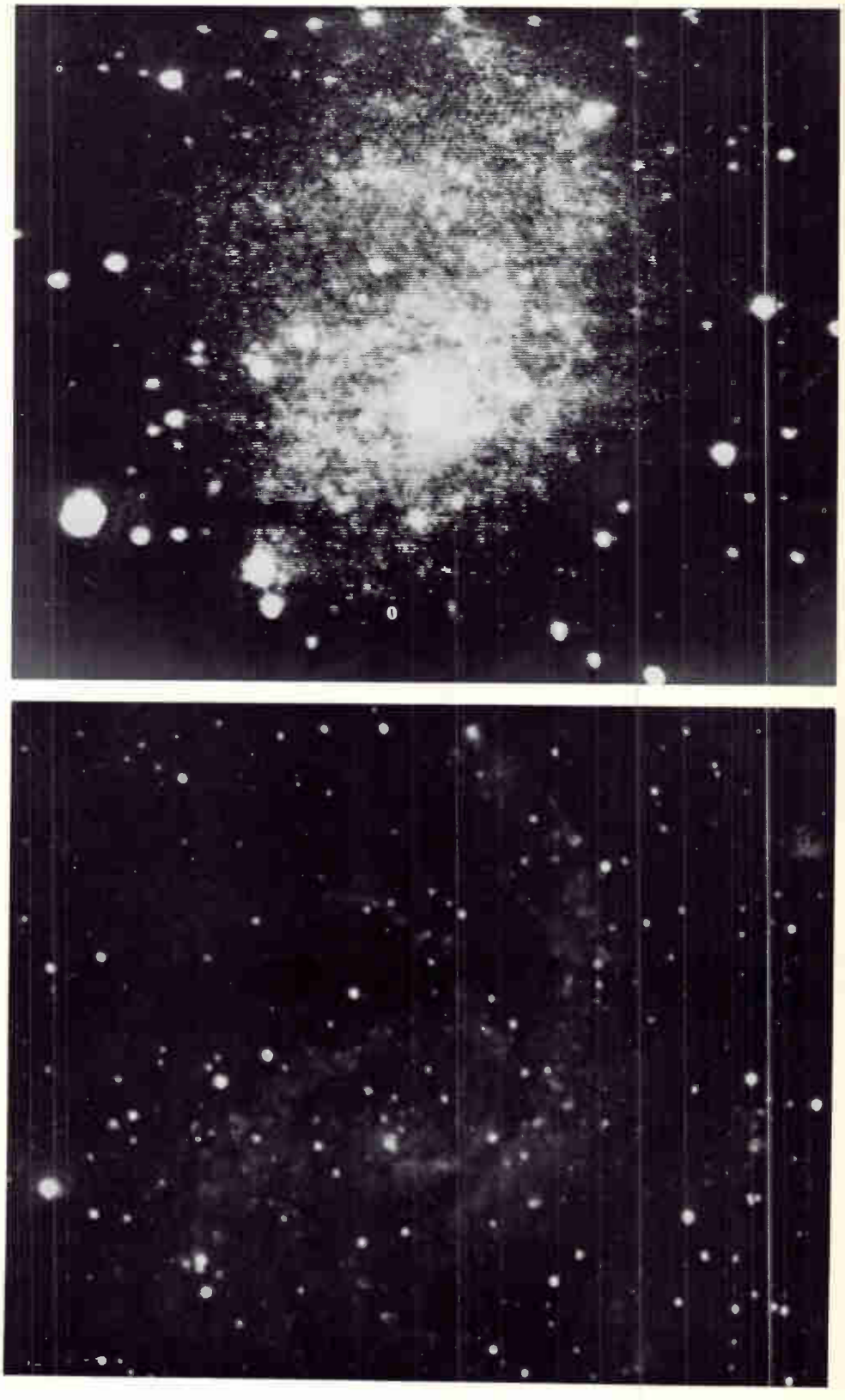

Westinghouse ENGINEER
March 1969, Volume 29, Number 2

Subscriptions: United States and possessions, $2.50 per year; all other countries, $3.00 per year. Single copies, 50¢ each.

Mailing address: Westinghouse ENGINEER, P. O. Box 2278, 3 Gateway Center, Pittsburgh, Pennsylvania 15230.

Published bimonthly by the Westinghouse Electric Corporation, Pittsburgh, Pennsylvania. Printed in the United States by The Lakeside Press, Lancaster, Pennsylvania. Reproductions of the magazine by years are available on positive microfilm from University Microfilms, Inc., 300 North Zeeb Road, Ann Arbor, Michigan 48106.

Cover design: A conveyor table, consisting of many rollers powered by individual permanent-magnet dc motors operating in unison, feeds steel to the rolling mill represented in Tom Ruddy's cover design. Permanent-magnet motors and their varied uses are discussed in the article beginning on page 46.

Probability Calculation of Generation Reserves

C. J. Baldwin

System planners have used probability methods extensively over the last ten years to solve their long-range generation planning problems. The most recent computerized approaches use continuous probability distributions of peak load and available capacity, rather than discrete values, to determine adequacy of generation reserves.

The application of probability methods to the long-range generation planning problem is most important to electric utilities committing large units for service with long lead times. Generation reserves at any given instant are affected by two chance or random events—forced outages of generator units on the system, and system load. Thus, generation reserve can never be predicted *exactly* for any specific time in the future. However, with appropriate probability techniques, utility planners can determine the system generation capacity required to provide reasonable assurance of maintaining a satisfactory generation reserve.

Forced outages of generator units are generally chance events. They occur for a variety of reasons in the steam generator, auxiliaries, prime movers, and the generator itself. Outages for any particular unit may be considered a sequence of random occurrences, which can be represented by a probability distribution. Analysis of historical data provides the basis for the probability representation of existing generating units. Forced outage predictions for new units must be engineering estimates of future performance.

Utility loads are random fluctuations about some mean system load, another probability distribution. With probability mathematics, the forced-outage and load probability distributions can be combined to determine the probability of not having sufficient generation reserves.

C. J. Baldwin is Manager of Development, Advanced Systems Technology, Westinghouse Electric Corporation, East Pittsburgh, Pennsylvania.

When long-term load forecasts of system planners are used for the calculation, *installed* reserve requirements are found from the probability combinations. If short-term forecasts of system operators and probabilities of their forecast error are used, *operating* reserves are determined. These two types of reserves are calculated for distinctly different purposes: The former indicates necessary generation purchases and installation schedules; the latter determines the required number of units to operate from a given complement of available units.

Probability Methods Using Discrete Values

The earliest application of probability mathematics to the generation reserve problem used the binomial expansion (see *The Binomial Expansion*). This technique provides a table of outage probabilities for discrete values of generation outage capacity, similar to Table IV. These outage probabilities are combined with a graphical expression of load variability, in the form of a daily peak duration curve (Fig. 1), to produce the so-called loss-of-load probability.[1]

Loss-of-Load Probability—The daily peak duration curve of Fig. 1 gives the number of weekdays of the year that the daily peak load will reach a certain value. The contribution to system loss-of-load probability (in days per year) for each outage of a particular magnitude (O_k in Table IV) is the probability of that outage (p_k) multiplied by the number of days (t_k) for which there will be a loss of load. The probabilities for all the various outage magnitudes (for the days of a given year) are summed to obtain a yearly loss-of-load probability. The binomial expansion is sometimes done on a monthly basis also, to account for the variations due to units scheduled out on maintenance. For large systems, however, a monthly binomial expansion increases computing time substantially and still allows only an approximate model of maintenance because it does not allow for maintenance periods shorter than one month.

Another fundamental shortcoming of the loss-of-load probability method is that it does not take into account the *uncertainty* of the forecasted annual peak in Fig. 1. The more accurate loss-of-load probability (P_i) is the summation of the expectancies of all deviations from forecast peak multiplied by the loss-of-load probability associated with each deviation: *Loss-of-Load Probability* $= \Sigma$ (*Proba-*

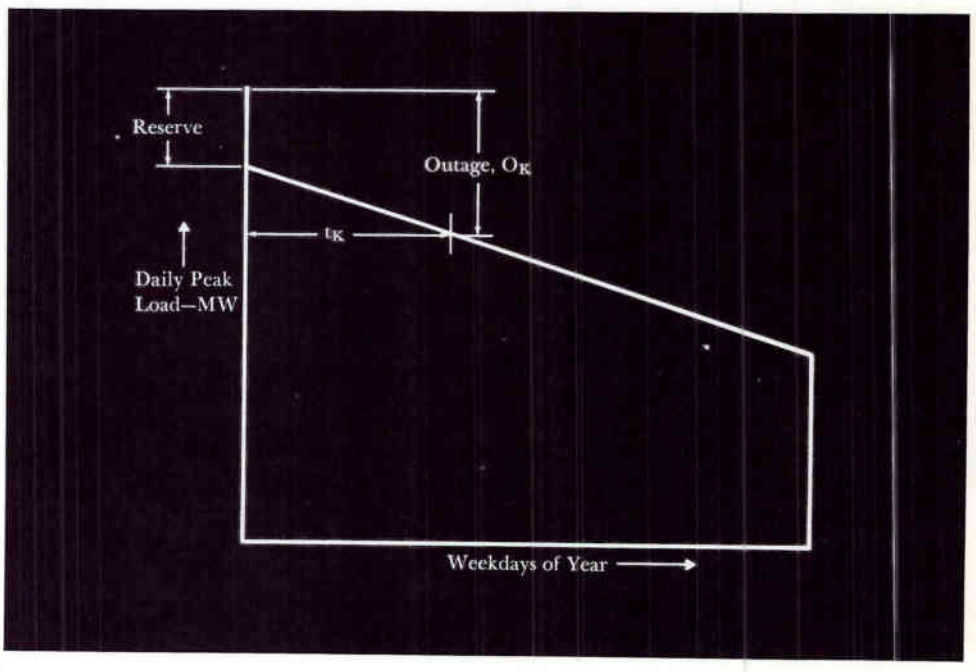

1—Daily peak duration curve gives the number of weekdays of the year that daily peak will reach or exceed a certain value.

The Binomial Expansion

The binomial expansion is one of the fundamental probability-generating functions used in probability mathematics. Applied to the generator outage problem, it uses the forced outage rate (p) for the units of a group (the probability of the existence of an outage on each unit) to predict the probability of any simultaneous combination of unit outages in the group.

The probability that a unit outage exists or does not exist must be unity. Thus, if the outage rate is p, then the probability that an outage does not exist must be $1-p=q$. For an n-unit group, each unit in the group having identical p and q probabilities, the probabilities for all possible combinations of unit outages are given by the binomial expansion,

$$(q+p)^n = q^n + nq^{n-1}p + n(n-1)q^{n-2}p^2 + \ldots + \frac{n!}{r!(n-r)!}q^{n-r}p^r \ldots + p^n$$

where r is the number of machines out of service at one time due to forced outages. Thus, the probability of exactly r outages is given by the $(r+1)$th term of the expansion,

$$\frac{n!}{r!\,(n-r)!}\,q^{n-r}p^r$$

which is the binomial probability function.

To illustrate the application of the binomial expansion, consider a hypothetical system consisting of four 20-MW units, each with an outage rate of 2 percent, and three 30-MW units, each with an outage rate of 2 percent. Considering first the group of four 20-MW units, $p = 0.02$, $q = 0.98$, $n = 4$, $r_1 = 0, 1, 2, 3$ and 4, the binomial expansion yields the outage probabilities,

$$(0.98 + 0.02)^4 = 0.922368 + 0.075296 + 0.002304 + 0.000032 + 0.00000016,$$

which are tabulated in Table I.

Similarly, the binomial expansion for the three 30-MW units gives the outage probabilities listed in Table II.

To determine the probabilities of combinations of 20-MW and 30-MW units being out simultaneously, the probabilities from Tables I and II must be combined in matrix form, as shown in Table III. For example, an outage of 0 MW on the system can only be obtained when both r_1 and $r_2 = 0$, so that the probability of a 0 MW system outage is $0.941192 \times 0.922368 = 0.868125$. Similar calculations are used to determine probabilities for other combinations of unit outages, as listed in Table III.

If system outages are considered in terms of megawatt capacity rather than specific units, there will be instances in which more than one combination of unit outages can produce the same total megawatt outage. For example, an outage of 60 MW can result from two 30-MW unit outages, or from three 20-MW unit outages. Therefore, the probability of obtaining a 60-MW outage must be the sum of the probabilities of the possible combinations; thus, from Table III, the probability of a 60-MW outage is: $0.000030 + 0.001085 = 0.001115$. The probabilities ($p_k$) of specific capacity outages are listed in Table IV.

For each step of outage capacity, the sum of the probabilities for all possible outages occurring must equal 1.0. Thus, the probability of an outage of 0 MW *or more* is a certainty and is therefore equal to 1.0. The probability of an outage of 20 MW or more will be the same as for 0 MW less the probability of an outage exactly equal to 0 MW. (The probability of an outage of 20 MW or more is also equal to the sum of all individual probabilities of outages equal to 20 MW and above.) In this way, the cumulative probability values (P_k) tabulated in Table IV were derived.

Table I. Outage Probabilities for 20-MW Units

Number of Units Out (r_1)	*Outage Capacity—MW*	*Probability of Outage*
0	0	0.922368
1	20	0.075296
2	40	0.002304
3	60	0.000032
4	80	Negligible

Table II. Outage Probabilities for 30-MW Units

Number of Units Out (r_2)	*Outage Capacity—MW*	*Probability of Outage*
0	0	0.941192
1	30	0.057624
2	60	0.001176
3	90	0.000008

Table III. Outage Probabilities for Combinations of 20- and 30-MW Units

		Three 30-MW Units			
	$r_1 \backslash r_2$	*0*	*1*	*2*	*3*
Four 20-MW Units	0	0.868125	0.053150	0.001085	0.000007
	1	0.070868	0.004339	0.000089	..
	2	0.002168	0.000133	0.000003	..
	3	0.000030	0.000002	..	..
	4	..	..	..	..

Table IV. Probabilities for Capacity Outages with 20- and 30-MW Units

Outage—MW O_k	*Probability of an Outage Exactly Equal to* O_k p_k	*Probability of an Outage Equal to* O_k *or More* P_k
0	0.868125	1.000000
20	0.070868	0.131875
30	0.053150	0.061007
40	0.002168	0.007857
50	0.004339	0.005689
60	0.001115	0.001350
70	0.000133	0.000235
80	0.000089	0.000102
90	0.000002	0.000013
100	0.000003	0.000011
110	..	0.000008
120	..	..

bility of Deviation)×*(Loss-of-Load Probability)*.

Outage probability is commonly expressed in years per day as either a monthly risk or an annual risk: *Monthly Risk (Years/Day)* = $1/12\ P_i$, *for Month i; Annual Risk (Years/Day)* = $1/(P_1+P_2+\ldots+P_{12})$, where P_i is the expected number of days in month i in which system peak load cannot be met. P_i can also be defined as the sum of the daily probabilities in month i of having zero installed reserve margin or less.

Note that annual risk is the average of all the monthly risks. The utility planner who bases his expansion plans on an annual risk of load loss should be careful that most of his annual risk is not being accumulated over a relatively small part of the year, perhaps the month or two during which his annual peak occurs. If this should be the case, a generation reserve planned on the basis of yearly risk could be in real trouble during the annual peak period.

Loss-of-Energy Probability, the expected per-unit energy curtailment, is an alternate measure of reliability. The method is similar to the loss-of-load technique except that the outage area under the load duration curve is calculated for each outage condition. This area times the probability of the outage, divided by the total area under the load duration curve, gives the energy curtailment on a per-unit basis. The various outage conditions are summed to get the expected per-unit energy curtailment on either a monthly or yearly basis.

Frequency and Duration of Outage is another method of expressing system reliability. The average expected frequency and duration of all possible forced outage conditions for the power system are determined. Unlike the loss-of-load method, where the probability of a particular outage *capacity* was found, this method separates the different ways that an outage can occur. For example, an outage of 60 megawatts can be obtained by loss of either three 20-MW units or two 30-MW units, which have outage probabilities of 0.000030 and 0.001085, respectively. Knowing this and the average down time for these unit sizes, the frequency of the outage occurring in a particular way is

$$D_r = P_r\left[\frac{r}{t}+\frac{(n-r)}{(1-p)T}\right]$$

where D_r is the outage frequency (times/year), P_r is the probability the outage will occur in a particular way, r is the number of units out, n is the total number of units, t is the average outage duration, T is the average interval between outages, and p is the average forced outage rate corrected for unit exposure by multiplying the unit forced outage rate by the fraction of the year the unit is in service.

The frequencies for the different ways a particular outage occurs are summed to get a total frequency of occurrence for that outage. After calculations have been made for all the different outage possibilities, the frequency of a capacity outage equal to or exceeding a specified amount can be found. Then the average duration of an outage of X or more megawatts is the probability of an outage of X or more megawatts divided by its frequency of occurrence. The interval between outages of X megawatts or more is merely the reciprocal of the frequency.

Knowing the annual peak, the installed capacity, and the capacity on maintenance during the month that the annual peak occurs, it is possible to plot annual peak load versus the duration of and interval between outages equal to or exceeding the effective reserve. If the calculation is terminated here, it does not allow for uncertainty of the load forecast nor variability of the daily loads.

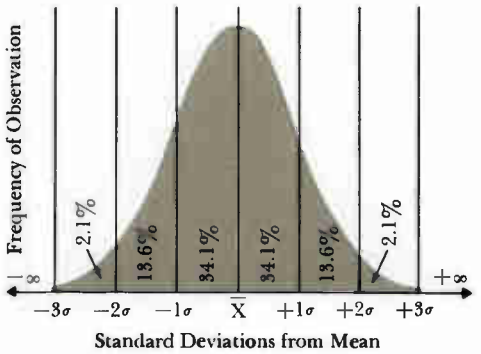

2—The normal distribution curve is based on one of the fundamental concepts of probability. This concept contains two principal postulates: (1) A variable (x) has a tendency to cluster about a center, or *mean* value ($\bar{x}$); and (2) individual readings will differ from the mean in a random but predictable pattern.

The amount by which the data differs from the mean value is expressed in terms of *standard deviation* (σ), which is the root mean square of the individual deviations from the mean, or:

$$\sigma = \sqrt{\frac{\Sigma\,(x_i - \bar{x})^2}{n}}$$

where x_i is each individual reading and n is the number of readings.

The standard deviation provides an indication of the dispersion (randomness) of data. If it is large in proportion to the mean value, the data varies widely; if small, dispersion is small, and a larger proportion of the data is near the mean value.

The standard deviation is an extremely useful means for analyzing data. For example, for a normal distribution, the probability of obtaining any particular range of deviations can readily be determined by expressing this range in terms of standard deviation units, and then comparing the area under the curve in this range to the total area under the curve (100 percent). For example, the probability of obtaining readings between plus two and plus three standard deviations is 2.1 percent.

Continuous Probability Distributions

To overcome the disadvantages of the older methods—no allowance for uncertainty of the peak load forecast nor realistic maintenance schedules—Monte Carlo simulation of discrete events was tried in the early days of digital computers.[2,3] While detail and accuracy were very satisfying, calculating time was not. However, the approach led to the development of a continuous probability distribution to represent loss of load. The more recent approaches in the application of probability mathematics to the reserve capacity problem differ from the

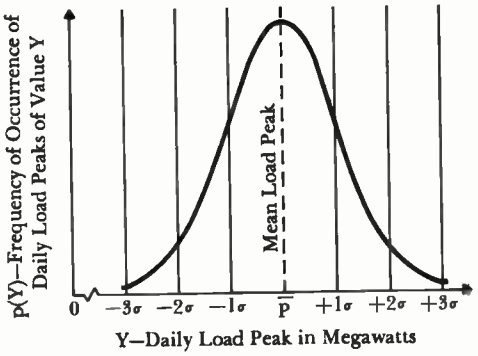

3—Daily peak loads can be described by a normal distribution curve.

Table V. Partial Table of First Order Statistic

Observations	*Mean Value of Highest Order Statistic*
5	1.16
10	1.54
15	1.74
18	1.82
19	1.84
20	1.87
21	1.89
22	1.91
23	1.93
25	1.97
30	2.04
40	2.16
50	2.25

Table VI. Effect of Load Truncation on Risk

Truncation Point in Standard Deviations Above Mean	*Years/Day Load Loss Risk*
13.0	6.06
5.0	6.06
4.5	6.06
4.0	6.08
3.5	6.16
3.0	6.45
2.5	7.66
2.0	9.29
1.5	12.1
1.0	18.0

earlier methods primarily in that they use continuous probability distributions of peak load and available capacity, rather than discrete values, and convolve these distribution curves mathematically to get a generation reserve margin distribution. The computation is fast because formulas can be used to accomplish the convolution. The most important advantages of the continuous variable approach are that it allows load peaks beyond the observed or forecasted peak to have a probability of occurrence, and thereby represents the actual situation more accurately, and it is fast enough to allow detailed unit maintenance planning on an equal-risk basis.

Load Distribution—The continuous variable method assumes that system load distribution is normal so that it can be described in terms of a *mean* daily load peak and a standard deviation (sigma) of load from this peak (Fig. 2). The mean and standard deviation values are characteristic of the load level and load variation in a certain month for a particular utility system or pool. Other months have distributions with other means and sigmas, depending on seasonal variations in level and fluctuation characteristics. Thus, the continuous variable method permits monthly loads to be described by just two numbers rather than cumbersome "daily peak load variation curves." Furthermore, the sigmas can be put in per unit of the mean so that certain generalities can be observed. For example, means and sigmas can be projected for future years by averaging or trending. As more systems are analyzed, means and sigmas appear to be predictable seasonally and geographically, at least within a range.

With normal distribution, daily load peaks can be viewed for a month as being say 21 (workdays of a month) draws from a large population having an underlying distribution whose properties can be estimated. The average of the 21 daily peaks provides a *sample estimate* of the underlying distribution mean. One of the 21 loads will be the largest of the group, representing the peak for the month. However, the calculation of load-loss probability must include the probabilities of having all possible loads from the normal distribution, which means including the probability of having load peaks higher than the one observed in the 21-day sample. The statistical relationship between the highest peak of the sample and the mean and sigma of the underlying distribution is given by the equation: *Estimated Value of Peak* = *Distribution Mean* + (*Distribution Sigma*) × (*First Order Statistic*), where the first order statistic is a constant determined by the number of draws in the group. This constant reflects the fact that the more draws in the group, the more chance for a higher observation. A partial listing of the first order statistic is shown in Table V. Using the first order statistic for a 21-day month from the table, the above equation says that if the distribution mean and sigma are known for the month, the best estimate of the peak is 1.89 sigma above the mean. Or, if the monthly peak is forecast, the best estimate of the mean of the daily peaks for the month is 1.89 sigma below the forecasted peak.

In computing probability of load loss with normal load distribution, a higher probability is obtained than when one assumes that the load distribution is truncated at the forecasted peak, which, for the monthly forecast, is only 1.89 sigma above the mean. A number of engineers (but rarely mathematicians) will argue that utility loads are in fact not normal because load can never exceed connected load, which certainly is not infinite. They argue that the load distribution should be truncated at connected load. The argument is valid, but the important question is the effect of truncation on risk, which is illustrated in Table VI. The table uses an exact binomial expansion for outages, which is then convolved with a normal load distribution with truncations at various sigmas above the mean load peak. For a 21-day month, the estimated value of the monthly peak is 1.89 sigma. If the load is truncated there (as in Fig. 1) rather than carried out to 3 or 4 sigmas, the years per day load-loss risk is optimistically biased by 50 or 60 percent. However, truncation beyond three or four sigmas (which is

certainly much less than connected load) is seen to have little further effect on risk. Hence, the conclusion is that truncation at any reasonable value is equivalent to using the full-tailed distribution.

A monthly load model based on normal distribution can be constructed for a power system as shown in Fig. 3. The daily weekday load peaks are used in groups corresponding to the separate months of the year. Long-term trends of annual peaks, seasonal factors, and the order statistics are used to establish the mean of the daily peaks, $\bar{P}$, and the standard deviation, σ_1.

Available Capacity Distribution—The probabilities of capacity outages, developed for discrete values by the binomial expansion, may be plotted as a continuous function as shown in Fig. 4. The mean forced outage ($\bar{L}$) is equal to $\Sigma p_i c_i$, where p_i is the forced outage existence rate for the ith unit and c_i is the megawatt capacity of the ith unit. The area under the curve represents probability and is unity. The standard deviation for the curve is

$$\sigma_2 = \sqrt{\Sigma p_i \, (1-p_i) \, c_i^2}.$$

The available capacity (X) is equal to the installed capacity (I) minus the forced outage capacity (L), or $X=I-L$, and can be plotted as the curve shown in Fig. 5. The mean available capacity ($\bar{A}$) is equal to the available capacity minus the mean forced outage ($\bar{A}=\bar{X}-\bar{L}$).

Margin Distribution—The margin of available capacity (M) is the available

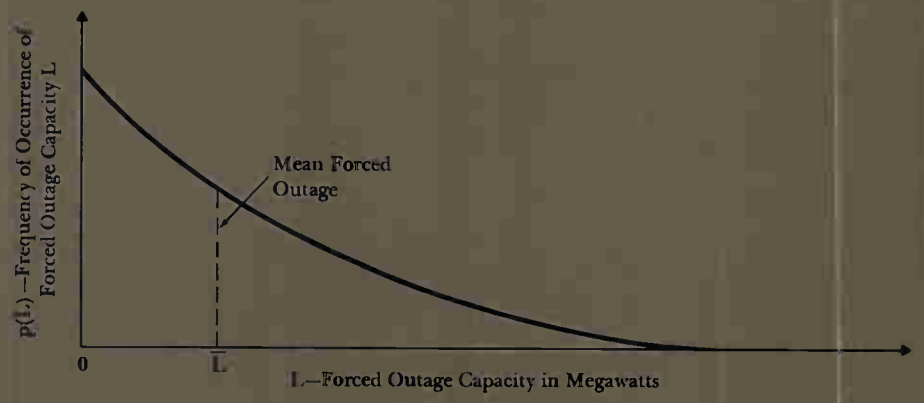

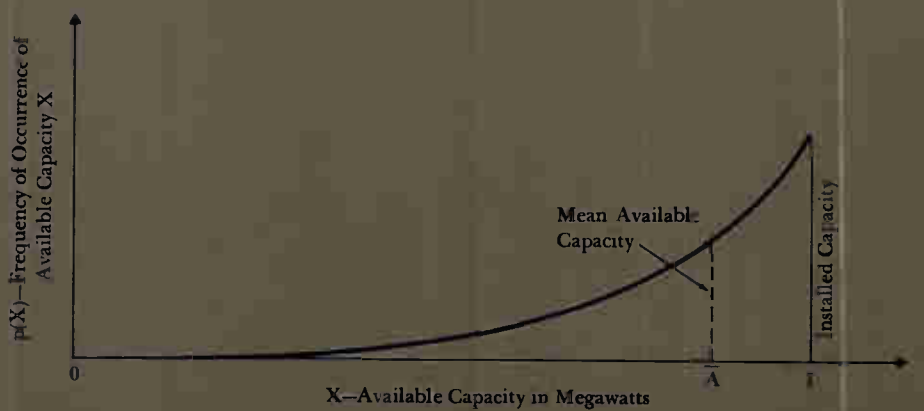

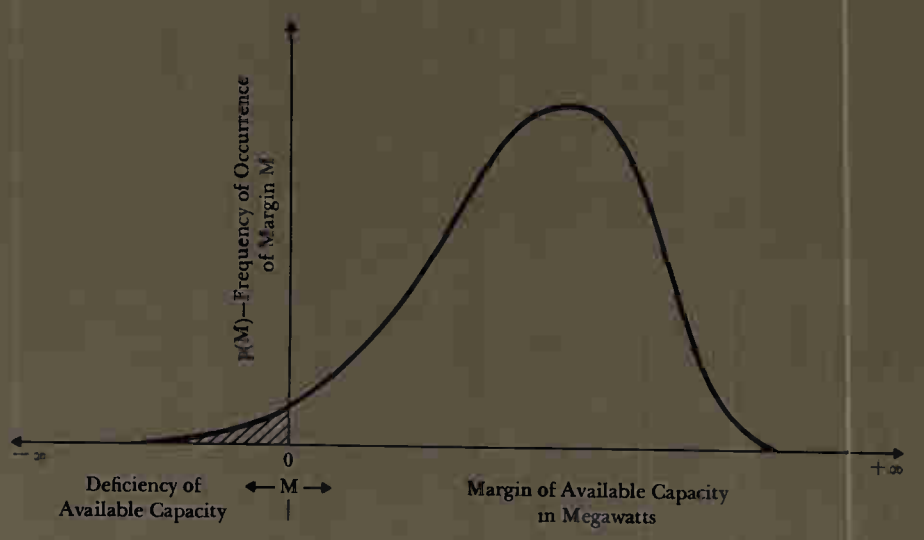

4—(*Top*) Probability of loss of capacity, developed for discrete values, can be plotted as a continuous function.

5—(*Center*) Available capacity curve is found by subtracting forced outage capacity (Fig. 4) from the installed capacity.

6—(*Bottom*) The margin of available capacity is found by convolving load and outage distributions (Figs. 3 and 5) with probability mathematics. The probability of zero margin or less is the area under the margin curve from $-\infty$ to 0, i.e.,

$$\int_{-\infty}^{0} p\,(M)\,dM.$$

System planners must decide what probability value is sufficient to provide reasonable assurance of maintaining satisfactory service.

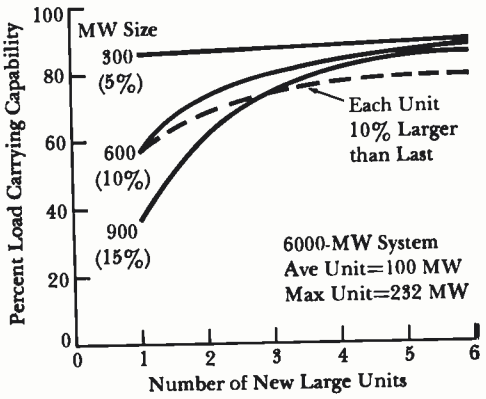

7—Load-serving capability as a percentage of the unit's rating for each of six subsequent larger new units installed on a sample system.

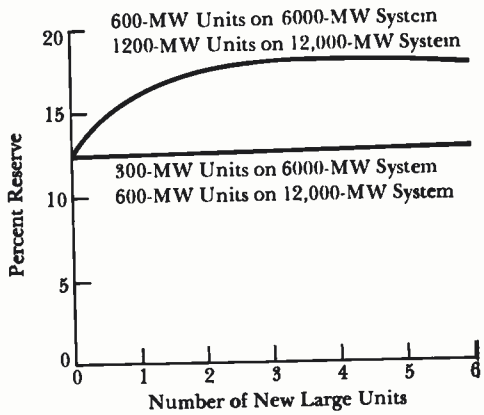

8—Percent installed reserve required for the total system as additional new large units are added in several sizes.

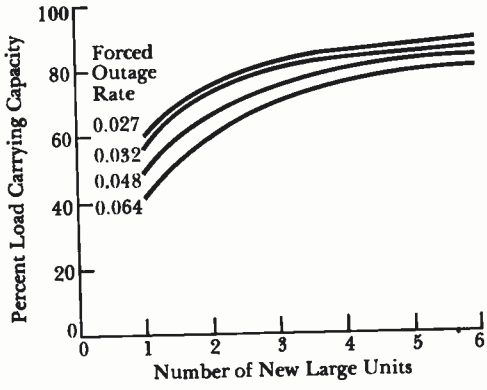

9—Load-serving capability as a function of forced outage rate of successive large 600-MW units installed on a 6000-MW sample system.

capacity less the load peak ($M=X-Y$). Thus, the load and outage distributions can be convolved with probability mathematics to get margin distribution, shown in Fig. 6. The mean of the margin curve ($\overline{M}$) will be the mean available capacity ($\overline{A}$) minus the mean peak load ($\overline{P}$), or $\overline{M}=\overline{A}-\overline{P}$. The standard deviation of the margin curve is the square root of the sum of the squares of the standard deviations for the outage and load distributions:

$$\sigma=\sqrt{\sigma_1^2+\sigma_2^2}.$$

Appropriate mathematical methods account for the nonnormality of the margin curve. The probability of negative margin, the shaded area in Fig. 6, is the probability that there will be a deficiency of available capacity to meet the peak load.

Load-Carrying Capability—An Application for Probability Calculation

One obvious source of economic savings on installed costs is the use of larger plants. However, the decrease in first cost of large plants is counterbalanced by the increased reserve requirement on any given system as unit size is increased; i.e., more capacity must be installed to maintain a given service quality because there are "more eggs in one basket." Another way to look at it is that if an unusually large unit were applied to an otherwise homogeneous system, a large part of its capacity must be assigned to reserve rather than peak load-carrying capability. When a second large unit of the same size is installed, less of its capacity must be assigned to reserve than was required for the first unit. This is in part because there is less probability of having two large units out at the same time. Similarly, a third large unit has even more of its capacity available to carry peak load.

Probability calculations can show how much of a unit's capability must be assigned to reserve when it is applied to any specific system. The amount depends upon the new unit's forced outage rate, existing unit sizes and outage rates, and the fluctuating characteristics of the system peaks. Calculations have been made for a number of typical systems, and Fig. 7 shows some curves of the load-serving capability of the first six large new units applied to a hypothetical 6000-MW system with an average installed unit size of 100 MW, a maximum unit size of 232 MW, and with relatively low outage rates and no allowance for peak load forecast error. The three solid curves show the load-serving capability of 300-, 600-, and 900-MW units, respectively. Expressed in percent of total installed capacity, these are 5-, 10-, and 15-percent units. Note that the first 10-percent unit has 43 percent of its capacity assigned to reserve, leaving only 57 percent available to carry growth in peak load. However, when there are two of these units on the system, the second has only 27 percent of its capacity assigned to reserve. Of course, the first unit is still caring for the largest single hazard. One might argue that part of the improvement in load-carrying capability is caused by the fact that the relative unit size is decreasing as the system grows and a 600-MW size is retained. However, the same general effect is seen if the unit size is allowed to increase along with the system growth. The dashed curve is for all 10-percent units; that is, the first unit is 600 MW, the second 660 MW, etc.

As successive 300-MW (5 percent) units are added, there is only a small increase in their load-serving capability. This is because the system reserve is already sized large enough to take care of nearly this big a hazard. Consequently, only the required reserve percentage for the total system, or about 12.5 percent, must be assigned to reserve on each new 300-MW unit.

Pooling offers a way to enjoy the lower installed costs of large plants without suffering as much penalty in load-carrying capability. The percent reserve requirements for a sequence of 300-MW, 5-percent units and 600-MW, 10-percent units applied to the same 6000-MW system is shown in Fig. 8. While 600 MW represents 10 percent of this system, it represents only 5 percent of a 12,000-MW system (also shown in Fig. 8). Thus, if the 600-MW unit were applied to the 12,000-MW system, it would enjoy exactly the same high load-carrying capability that

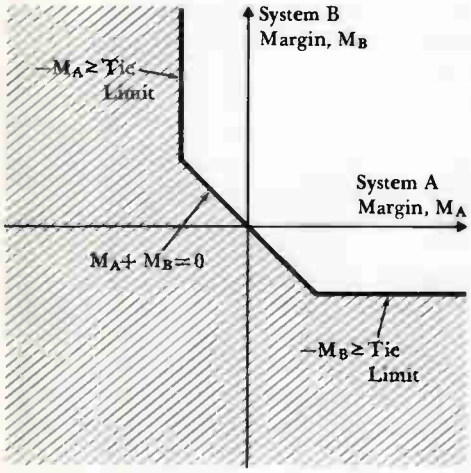

10—The improved margin for the integration of two systems with tie limitations is indicated by the unshaded area outside the upper right-hand quadrant.

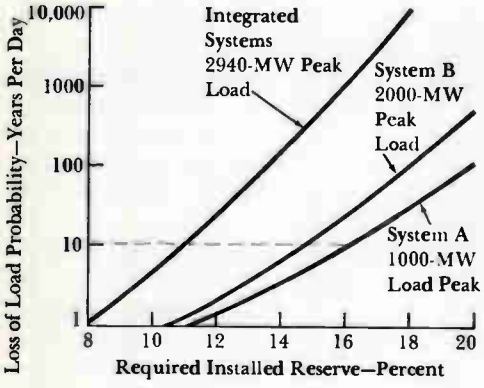

11—Reserve savings from pooling of two utility power systems as a function of service quality maintained.

the 300-MW unit has on the 6000-MW system. Similarly, the 600-MW curve on the 6000-MW system applied to a 1200-MW unit on the 12,000-MW system. These statements assume no increase in forced outage rate with increase in size. If forced outage rate increases with size, as many believe it does, there would be some loss in load-carrying capability and greater reserves required. The amount is demonstrated in Fig. 9 for 600-MW units on the 6000-MW system. However, the fact remains that a large unit's load-serving capacity can be greatly improved by scaling up system size.

The discussion so far has dealt with reliability calculations for a single company or single completely integrated pool. As large pools become an operational reality, a logical consideration is the economy to be realized by further coordinated planning and operation among neighboring pools. This step introduces the problem of pool-to-pool studies. An additional question of importance in these studies is how much interconnecting transmission capacity is required to effectively pool the two pools. Probability techniques have been extended to permit the solution of this problem. The load and capacity distributions of each pool must be included. Probability calculations are made for each pool, recognizing the margin situation in both. The improved margin for the integration of two systems with tie limitations is illustrated in Fig. 10. The shaded area indicates negative margin for the integrated pools with tie limits. If systems *A* and *B* were not interconnected, all but the upper right-hand quadrant would represent negative margin.

In pool-to-pool calculations, tie capacity is permitted to have different ratings for export and import as might be caused by transmission limitations within each pool. Limits may be imposed on the amount of tie built to represent physical or contractual limitations. Finally, load correlation, the degree to which daily peak fluctuations occur simultaneously in the two pools, must be accurately included. A high degree of load correlation has an adverse effect on the risk. For example, when pool *A* needs tie help because a heat wave has driven up the cooling load, it might be that pool *B* is unable to supply reserve generation because the same weather has had a similar effect on its load.

The reserve savings that can result when full advantage is taken of ties between systems or pools is illustrated in Fig. 11. At ten years per day risk, the required reserve drops from 15 and 16 percent of individual peaks to 11 percent of the coincident peak, while service quality remains at the same level.

Conclusion

This discussion has dealt with several methods of applying probability mathematics to the calculation of generation reserve requirements. The binomial expansion requires analysis of discrete variables to which several measures of reliability, such as loss of load, loss of energy, and frequency-duration may be applied. However, the more recent representation of system load and available capacity by continuous functions has several advantages over the discrete-variable methods. The familiar loss-of-load probability index as a service quality criterion can be retained, but computation is faster and can be readily adapted to a variety of planning problems such as maintenance planning, tie representation, and pooling.

The evolutionary trend in the application of probability methods to generation planning has not yet run its course. The need for more sophisticated long-range plans and the availability of larger and more powerful digital computers have set the stage for significant advances in all phases of power system reliability analysis.

REFERENCES:

[1] "Applications of Probability Methods to Generating Capacity Problems," AIEE Committee Report. *AIEE Transactions*, vol. 79, pt. III, 1960. pp. 1165-1182.

[2] "Mathematical Models for Use in the Simulation of Power Generation Outages—I, Fundamental Considerations," C. J. Baldwin, D. P. Gaver, C. H. Hoffman. *AIEE Transactions*, vol. 78, pt. III, 1959, pp. 1251-58; "II—Power System Forced Outage Distributions," C. J. Baldwin, J. E. Billings, D. P. Gaver, C. H. Hoffman. Ibid, pp. 1258-72.

[3] "System Simulation . . . For Aiding Utility Planning and Operation," J. K. Dillard and C. J. Baldwin, *Westinghouse ENGINEER*, Sept. 1960, pp. 130-5.

AC Power Provides Flexible Maneuvering for Deep-Submergence Rescue Vehicle

Robert C. Fear
Robert R. Madison
Joseph M. Urish

The U.S. Navy's Deep Submergence Rescue Vehicle will require precise positioning capability for its missions. Battery-powered ac systems for propulsion, maneuvering, and hydraulic equipment provide that capability.

When the first Deep Submergence Rescue Vehicle (DSRV) is completed this year, the U.S. Navy will have a rescue vessel able to reach disabled submarines at depths to 3500 feet. Carried to the vicinity by a "mother" submarine, the DSRV will maneuver under its own power to locate the disabled submarine and attach itself to the escape hatch; then it will rescue 24 men in each trip to the mother submarine. When not needed for rescue duty, the vessel will be used for scientific tasks such as ocean floor mapping with sonar.

Because speed is essential in rescue operations, the DSRV must be small and light enough to be carried by jet transport to any place in the world. At the same time, its pressure hull and external systems must be strong enough to withstand the crushing water pressure of the ocean depths, which reaches 2250 psi at 5000 feet, the eventual operating depth of the DSRV.

The DSRV also needs precise navigating and maneuvering capability to enable it to locate and mate with the disabled submarine quickly. Requirements are considerably more demanding than those of conventional submarines, because in a rescue operation the vehicle's position must be controlled within inches despite strong water currents and low vehicle speed (which makes conventional controls sluggish or ineffective).

The Navy has incorporated a navigation system that can be used either as an accurate dead-reckoning system or, with sonar, as a precise navigation system referenced to the sea floor. For carrying out the required maneuvers, the Westinghouse Aerospace Electrical Division has designed and supplied systems for propulsion, maneuvering, and hydraulic power. The engineering principles of the systems are extensions of those successfully applied in the deep-submergence research vehicle *Deepstar 4000*.

Robert C. Fear is Manager, Deep Submergence Programs, Aerospace Electrical Division, Westinghouse Electric Corporation, Lima, Ohio. Robert R. Madson and Joseph M. Urish are design engineers there.

General Description

The DSRV propulsion and maneuvering system is composed of one 15-horsepower main propulsion drive system, four 7½-hp thruster drive systems, and two 7½-hp hydraulic-pump drive systems. The propulsion drive system powers a six-foot propeller at the rear of the vehicle, and each thruster drive powers one of the maneuvering propellers oriented laterally and vertically at the front and rear of the vehicle. The hydraulic-pump drives provide hydraulic pressure to actuate various controls and pump systems. Each drive system consists of a solid-state controller and an ac motor unit (see Table I).

For rapid travel to rescue depth, the propulsion system can be made to deliver 20 hp instead of 15 hp by increasing the controller output frequency 10 percent (to 66 hertz). Such operation imposes thermal overloads in the controller, so it is restricted to 10 out of every 30 minutes.

The controllers operate over an input voltage range of 100 to 140 volts dc from the vehicle batteries. Each is enclosed in a spherical pressure vessel, allowing its components to operate in a controlled environment.

Propulsion and thruster motor units include gearboxes. The units are filled with fluid and pressure-compensated to allow for changes in fluid volume with external water pressure and changing temperature. The hydraulic-pump drive motors operate submerged in the vehicle's hydraulic fluid, and they do not have gearboxes. All motors are designed to operate in ambient pressures up to 2250 psi.

Motor, gearing, and controller are connected into a complete propulsion or thruster system as shown in Fig. 1. A contactor at the battery bus, remotely operated from the crew compartment, opens and closes the battery input circuit. Control signals from equipment in the crew compartment adjust controller output frequency and phase sequence to control motor speed and direction of rotation.

The hydraulic-pump drive systems are controlled simply by on-off switches, since neither adjustable speed nor reversibility is required.

Controllers and motors are constructed for continuous operation at seawater temperatures between 28 and 85 degrees F. The systems can be operated in air for five-minute checkout periods. When not operating, the systems can be exposed to continuous temperatures of −40 to 160 degrees F with no detrimental effect.

The equipment is built to withstand shocks that may occur during shipping, installation, launch, or operation in rough seas (wave slap up to 1000 pounds per square foot). Motors and controllers are designed for 10-year life and 2000 submergence cycles.

Table I. Main Characteristics of DSRV Drive Systems

Characteristic	*Propulsion System*	*Thruster Systems*	*Hydraulic-Pump Systems*
Weight of Motor Unit and Controller in Air (lb)	508*	279*	247
Displacement (ft^3)	3.94	2.5	2.1**
Efficiency at Full Load (%)	60	60	70
Rating (shp)	15***	7.5	7.5
Output Speed (r/min)	2 to 90***	12 to 590	3450
Motor Reversing Time (full speed in one direction to 90% speed in reverse direction) (sec)	3.5	3.5	Not reversible

*Includes coolant fluid in motor and gearing unit.
**Controller only. Motor is immersed in fluid of hydraulic system.
***Operable at 98 r/min and 20 shp for limited periods.

Controllers

Electrical Design—Each controller consists of a static dc-to-ac three-phase adjustable-frequency inverter. (See Fig. 1 and Table II.) The inverter employs front-end commutation (bridge commutating action accomplished at the dc input) and digital control to convert dc input power to three-phase variable-frequency output power. Six heavy-duty thyristors are connected in a standard three-phase inverter bridge that does not require interphase transformers or reactors to supply power suitable for a polyphase induction motor. Proven solid-state digital control circuitry provides wave-form and frequency control to prevent motor saturation under various conditions of load and battery voltage.

The thruster and main propulsion controllers are regulated from the operator's panel, which provides signals for *start*, *stop*, *rotational direction*, and *speed*. The *start* function applies power to the controller in such a way as to insure that commutating conditions and control logic pulses have been established. Motor speed is regulated by frequency control through a feedback loop, and rotational direction is determined by control of phase rotation. Signals from the motor actuate indicators of speed and direction of rotation in the crew compartment.

The controller is started by closing the battery contactor; opening the contactor shuts down the controller and resets it for the next start. An overtemperature or overload condition clamps the thyristor firing circuits off, reducing current into the controller. An indicator light alerts the operator to either condition, and he must reset by commanding zero speed and then returning the speed control to the desired setting.

Control circuits are composed of solid-state digital elements. Two feedback signals from the inverter output control the output wave form. The first signal is a measure of the volt-seconds per cycle of the output wave form, and the second is the dc line current into the output bridge. The first signal controls the output voltage to maintain constant volts per cycle or a controlled volts-per-cycle increase applied to the motor as frequency is decreased. The second signal provides an adjustable current limit to protect the motor and controller components.

For overload protection, the current feedback loop provides a signal to a clock module that limits the peak dc line current to a value the commutating circuit can reliably accommodate. This protection controls the peak currents that occur during motor starting, plug reversing, or locked-rotor conditions.

Controller components were selected for high reliability. The calculated mean time before failure for the prototype controller is more than 10,000 hours. Recommended maintenance involves only periodic replacement of filter capacitors and commutating capacitors. The logic control circuits consist of five printed circuit boards, all of which have plug-in connectors for ease of replacement. All other components are readily accessible and can be removed with ordinary hand tools.

Mechanical Design—The major design objectives were to protect the controller components from the high water pressures encountered at operating depths, to provide sufficient cooling to limit component temperatures to conservative levels, and to make the electrical components easily accessible for maintenance. Those objectives have been achieved by mounting all components and modular assemblies on an aluminum-alloy base plate, then sandwiching the plate between two hemispherical heads (Figs. 2 and 3). The base plate acts as a heat sink through which component losses are conducted out to the edge, which is exposed to seawater. (This mounting arrangement is used successfully in the five-kW controller for *Deepstar 4000*.)

The hemispherical heads are clamped against the base plate and sealed by O-rings. The interior is maintained at essentially sea-level pressure, so water pressure at operating depths forces each head against the sealing surface to effect a leak-free seal.

The pressure heads are of aluminum alloy, with walls 0.592 and 0.520 inch thick for the two sizes (20- and 17-inch

Table II. Controller Characteristics

Characteristic	*Propulsion Controller*	*Thruster and Hydraulic-Pump Controllers*
Input Voltage (V dc)	100 to 140	100 to 140
Output Voltage, Line to Line (V ac, rms at 60 Hz)	82	82
Frequency (Hz)	0 to 60*	0 to 67**
Efficiency at Full Load (%)	90	90
Life Expectancy (years)	10***	10***
Size, OD (in., major/minor)	24.0/21.9	21.3/19.3
Weight in Air (lb)	270	189

*Frequency is 66 hertz at 20 shp.
**Hydraulic-pump controllers provide 60 Hz only.
***Ten-year life is achieved by periodic replacement schedule. Electrolytic filter capacitors and commutating capacitors will be the major components concerned.

1—Deep Submergence Rescue Vehicle (DSRV) propulsion system converts battery power into adjustable-speed motor output. The controller is essentially an inverter that supplies adjustable-frequency ac power to the squirrel-cage motor. System indicators and controls are located inside the crew compartment. The systems for the vessel's four thrusters are similar to the propulsion system, though of lower rating; those for the two hydraulic-pump drives have similar controllers and motors but need no gearing nor provision for controlling motor speed and rotational direction.

***Right*—Artist's concept of the DSRV being built by Lockheed Missiles and Space Company. The vehicle is shown mating to the restraining guide wires and "piggyback" berth on its mother submarine. A large propeller at the aft end provides propulsion, and smaller propellers in vertical and horizontal thruster ports at bow and stern provide maneuvering thrust.**

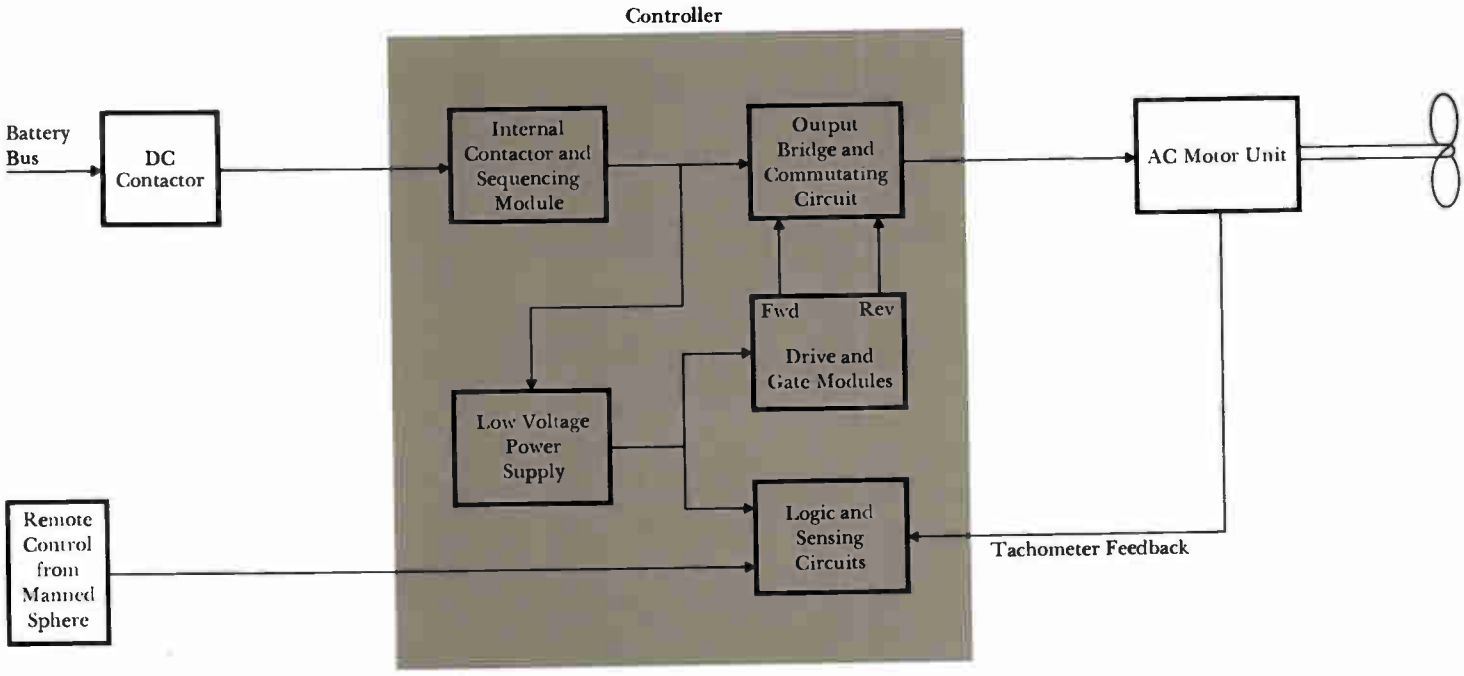
Controller
Battery Bus
DC Contactor
Internal Contactor and Sequencing Module
Output Bridge and Commutating Circuit
AC Motor Unit
Fwd
Rev
Drive and Gate Modules
Low Voltage Power Supply
Logic and Sensing Circuits
Remote Control from Manned Sphere
Tachometer Feedback

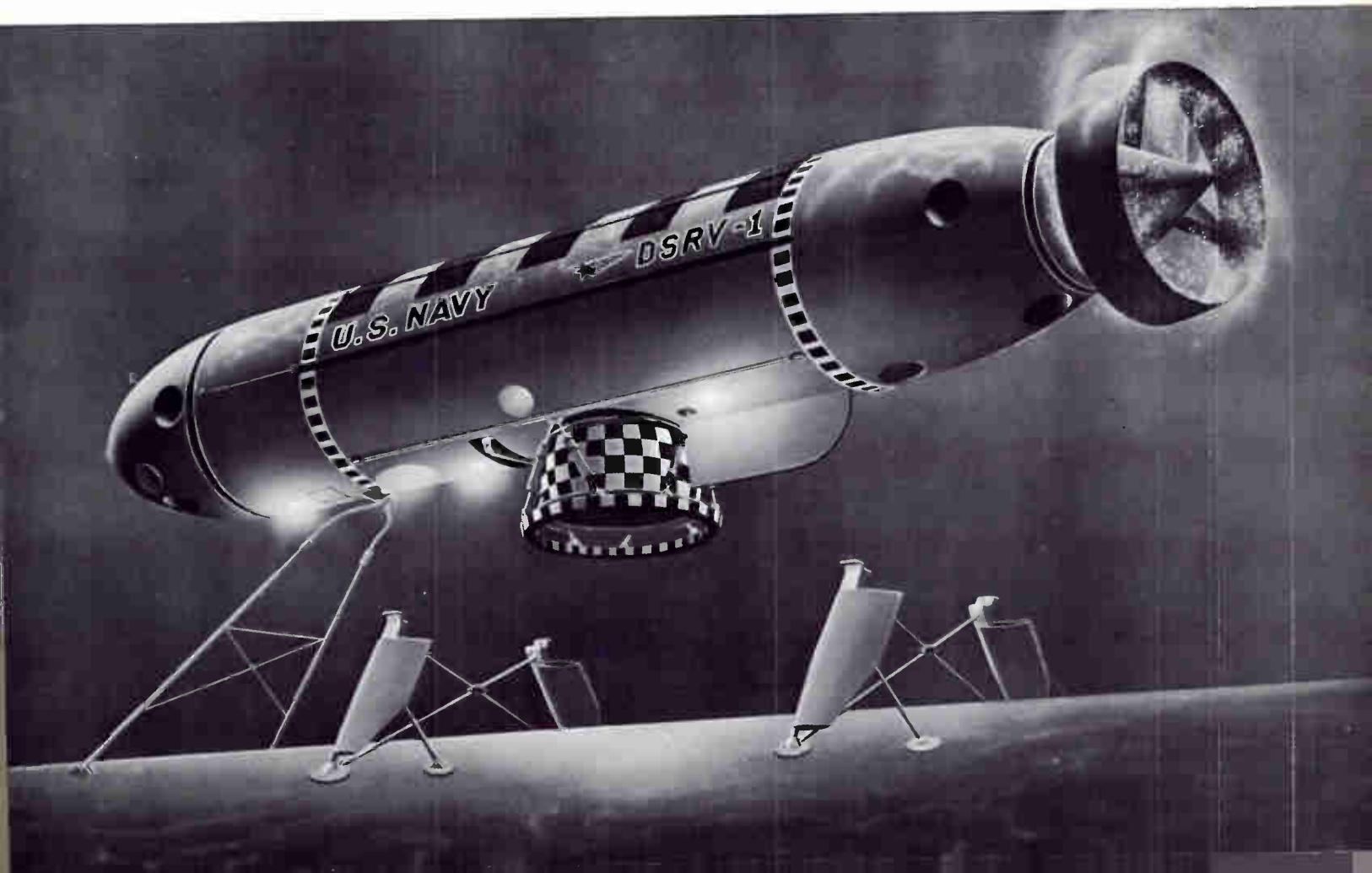
U.S. NAVY
DSRV-1

2

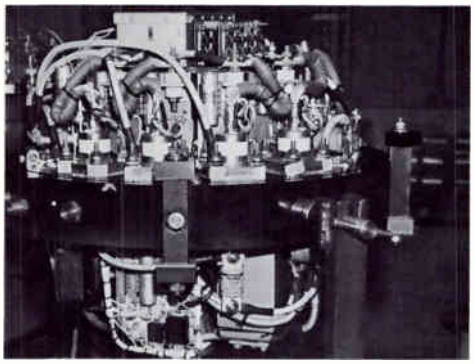

3

4

5

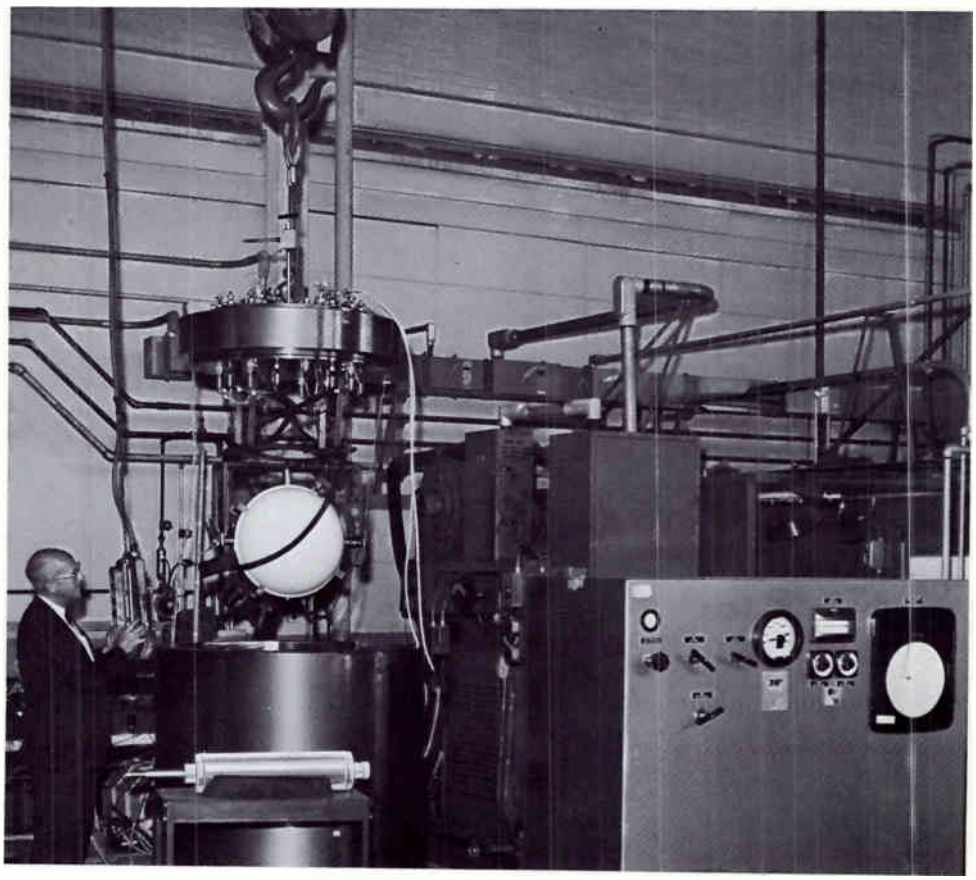

2—Thruster controller (with covers removed) has components mounted on a base plate that serves as a heat sink.

3—Propulsion controller shown with covers installed. Covers are hemispherical pressure vessels that protect the controller components from the great pressure at operating depths. The technician is installing electrical cables before a pressure test.

4—Thruster motor unit (shown here) and propulsion motor unit are similar except that the latter is larger. The units consist of a motor and reduction gearing enclosed in a housing, which is filled with a coolant fluid pressure-compensated to allow for changing outside water pressure and for thermal expansion. Thruster motor top speed of 3450 r/min is reduced by the gearing to 590 r/min shaft speed

5—Controller mounted on the cover of the Aerospace Electrical Division's pressure test chamber is about to be lowered into the chamber. (A thruster motor is on the cart in the foreground.) The chamber is filled with salt water; a pressure of 13,500 psi can be attained in 30 minutes pumping time. The test chamber is three feet in inside diameter by six feet in inside length. The cover has sixteen 200-ampere electrical power penetrations and 24 thermocouple penetrations. Motor units as well as controllers have been operated in the facility under pressures exceeding the service operating pressures.

inside diameter, respectively). This construction minimizes vessel weight and size, for buoyancy and ease of transporting, while retaining adequate strength. The vessels are designed for operation at 2250 psi, and they withstand a collapse-test pressure of 3500 psi (pressures equivalent, respectively, to 5000- and 7800-foot depth).

Cable Connections

Water-tight connectors are used at the cable entrances of controllers and motors; they are designed for operating pressures up to 13,500 psi. The molded cable assemblies will be blocked to seawater entrance at both ends.

Propulsion Motor Unit

The motor and its speed-reducing gear train are enclosed by an aluminum housing. (See Fig. 4 and Table III.) It is filled with a synthetic organic fluid for cooling and exclusion of seawater; the fluid is retained by a face-type rotating shaft seal.

Electrical Design—The two-pole ac squirrel-cage induction motor operates at 3450 r/min with a 15-hp propeller load on a 60-hertz electrical input. Synchronous speed is 3600 r/min with 60-hertz input and 120 r/min with 2-hertz input.

The motor is designed for 82 volts line to line at 60 hertz. Stator windings are delta connected to match the inverter and provide the best system efficiency; the delta connection also allows use of a smaller wire size with more turns per coil than a "Y" connection, resulting in a more compact winding for the chosen voltage rating.

Stator winding wire is insulated with an enamel thickness of two mils per side, providing compactness, good heat transfer from the wire to the surrounding oil, and protection for a limited time from direct seawater immersion. Stator slot cells are a laminate 10 mils thick. The wound stator is vacuum-impregnated in varnish to maintain winding rigidity when subjected to vibration and to provide additional protection against short-time exposure to seawater. This insulation system was subjected to short-time cyclic static pressure tests in fresh water at 20,000 psi without detectable degradation. It has also been operated successfully in an engineering feasibility model tested to 13,500-psi pressure at the Aerospace Electrical Division test facility; the fluid fill was diluted 10 percent with salt water for a 50-hour test period.

Mechanical Design—The motor is mounted in the aluminum housing with clearance over the stator frame to provide room for circulation of the coolant fluid and to equalize fluid pressures on both ends of the rotor. Sleeve bearings support the rotor.

The planetary gearing style was selected for light weight, high capacity, reliability, and high efficiency. Helical gears are manufactured with precision shaping equipment for accurate involute profile and spacing. The high-speed sun gear is made from carburized SAE 8620 material and is integral with the motor shaft. Planetary gears are through-hardened SAE 4140 material and are mounted on hard steel journals operating in replaceable bushings in a ductile-iron carrier. The internal ring gear is made of SAE 4140 through-hardened material and is mounted on a ductile-iron web to the output shaft, which is supported by tapered roller bearings to withstand propeller thrust and wave slap.

Effects of Seal Leakage—A small quantity of seawater can be absorbed by the cooling fluid. Additional water over that which can be absorbed does not form a thick "mayonnaise" emulsion as it does with some hydrocarbon fluids. Partial or total replacement of the fluid by seawater would increase fluid density and viscosity, resulting in greater fluid friction losses; however, the unit would operate for a period exceeding mission time.

Rotor and stator assemblies would not be affected by short-term saltwater ingestion, though longer exposure would cause corrosion. The effect of seawater on the primary conductor insulation would be to increase electrical leakage eventually; electrical components might have to be replaced. The remaining components would be salvageable, except for the component that permitted the gross entrance of seawater.

Other Motor Units

General construction of the thruster motor units is the same as that of the propulsion unit. (See Fig. 4 and Table III.) The motor shaft is machined with a gear on one end for driving the propeller gearing of the thruster unit and with a spline on the other end for driving the hydraulic pump; thus, rotors are interchangeable. The pump motor units have no reduction gearing.

Conclusion

The DSRV will give the U.S. Navy the capability for worldwide rapid submarine rescue. System requirements to achieve that capability are even more demanding than those of conventional submarines: besides the requirement for small size to permit air transport to the point of need, the DSRV demands precise maneuvering and propulsion control for locating a disabled submarine and mating with its escape hatch. The advanced solid-state control systems and the compact motor and gear units help meet both requirements.

Table III. Motor-Unit Characteristics

Characteristic	*Propulsion Drive*	*Thruster Drives*	*Hydraulic-Pump Drive*
Motor Power Factor at Full Load	0.9 lag	0.9 lag	0.9 lag
Weight in Air (lb)	238*	90*	58
Displacement (in.^{3})	1870	670	227
Overall Length (in.)	52.75	30.2	15.75
Mounting Flange Diameter (in.)	16.0	No flange	6.750
Motor Diameter (in.)	7.5	6.0	5.250

*Includes coolant fluid.

The Modern Permanent-Magnet DC Motor

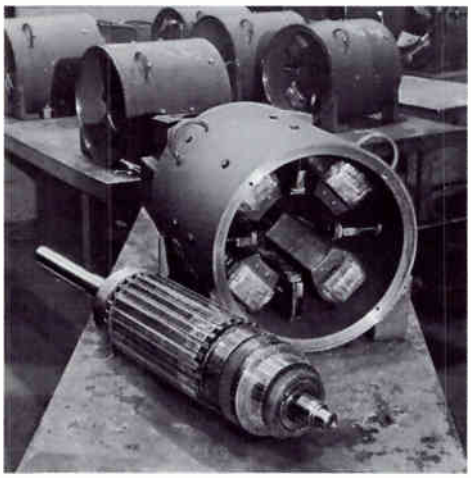

1—Permanent-magnet motors in integral-horsepower sizes have Alnico magnets for the main poles. (The smaller poles are wound commutation poles.) Windings around the main poles are for magnetizing and demagnetizing the permanent magnets.

Recent improvements in magnet materials have given permanent-magnet motors high capability and new application flexibility.

Permanent-magnet dc motors differ fundamentally from wound-field dc motors in that current need be supplied only to the armature, while wound-field motors require current for both the armature and the field windings. That difference in design influences both motor performance and overall cost.

Elimination of field excitation, for example, increases efficiency, simplifies control, and reduces maintenance requirements. It also reduces installation costs by reducing the amount of wiring needed. Speed drift caused by temperature change is much less than with wound-field motors, and overload torque per ampere is higher. Moreover, the low armature inertia of the Westinghouse permanent-magnet dc motors reduces the amount of power required for acceleration and provides the faster response speed that has become so useful in many modern industrial drive systems.

The first permanent-magnet motors in integral-horsepower sizes were made by designing the magnets to suit existing motors, so the magnet size was limited by existing armature and frame dimensions; as a result, the motors operated at lower than desired flux levels and had low peak torque capability. Changing the approach by designing the motor to suit the permanent magnet resulted in the present Westinghouse high-performance motors.

The earlier permanent-magnet motors in integral-horsepower sizes also were severely hampered by the low energy level of the magnets then available; the flux level that could be obtained was not high enough to allow the motor to compete economically with conventional wound-field dc motors for general applications. Joint development work with various suppliers of Alnico permanent magnets improved the energy level until, by 1960, it became possible to build permanent-magnet motors to compete economically with wound-field motors for many applications. And since then, the energy level of the magnets has been increased more than 25 percent, so the present motors work at higher air gap flux densities than do wound-field motors.

James C. Wachob is a product design engineer and John C. Erlandson a design engineer in the computer section, Large AC/DC Motor Division, Westinghouse Electric Corporation, Buffalo, New York.

Design of Permanent-Magnet Motors

In the permanent-magnet motor, each main pole is an Alnico magnet that produces the motor's flux (Fig. 1). Although ceramic magnets cost much less than Alnico magnets and are used in fractional-horsepower motors, they can produce only a third of the flux that Alnico magnets produce. Integral-horsepower permanent-magnet motors need high flux levels to compete with wound-field motors, so Alnico magnets are used.

Normal temperature, vibration, or aging do not cause an Alnico permanent-magnet motor to lose flux. The flux output of the magnets does not change with temperature until the magnet reaches 300 degrees C, and that is more than double the maximum permissible temperature for Class B insulation. Heavy and repeated shocks do not cause the permanent magnets to lose flux; mechanical failure would result before any loss in flux were detected. As for aging, a magnet supplier has estimated that the Alnico magnet will lose less than one-half of one percent of its flux level in two thousand years.

However, the permanent-magnet main poles do lose flux if the motor is loaded beyond its design limit. The loss in flux gives the motor new electrical characteristics, such as higher speeds and less torque per ampere. Flux loss from overloads can be calculated the same as other motor characteristics. (See *Calculating Motor Flux*, page 48.) Once a motor loses flux from a given overload, it does not lose additional flux until the motor is overloaded beyond its previous maximum overload. The amount of flux the motor loses from an overload varies with the motor design and magnitude of overload. Once a motor loses flux, it can only be brought back to the original flux level by re-energizing the magnets, but that is

done simply by energizing the motor's excitation coil for two seconds.

The only other known way in which a permanent-magnet motor has lost flux is when a strong magnet, such as the electromagnets used on overhead electric cranes, touches the motor frame. The flux from the electromagnet may saturate the frame and cause a loss in motor flux level.

All Westinghouse permanent-magnet motors are so designed that they will not lose flux until they reach their commutation limits at base speed, which means they have high overload capability without loss in flux. That capability is achieved by making the permanent-magnet main poles radially longer than equivalent wound-field poles. Since it is desirable to retain standard mounting dimensions, the use of large poles requires the armature diameter to be smaller than that of equivalent wound-field armatures. However, permanent-magnet motor armatures must have the same volume (D^2L) as the equivalent wound-field armatures to produce equivalent overload peak torques, so permanent-magnet motors usually have long armature cores. Ratio of armature length to armature diameter varies between 2 to 1 and 4 to 1, while in wound-field motors the ratio varies between ½ and 1½ to 1. The small diameter results in one of the lowest-inertia motor lines in industry (Fig. 2).

Standard dc motor design practices are used for permanent-magnet motors. Extreme care must be given to all portions of the magnetic circuit because, if any portion of the circuit saturates prematurely during overloads, the saturation can cause a premature loss in flux. The procedure used to calculate the motor's flux is described in *Calculating Motor Flux*, page 48.

Commutation problems are similar to those of any dc motor. Most permanent-magnet motors require conventional wound-field commutation poles to commutate successfully.

Before development of computer design programs, the engineer had to de-

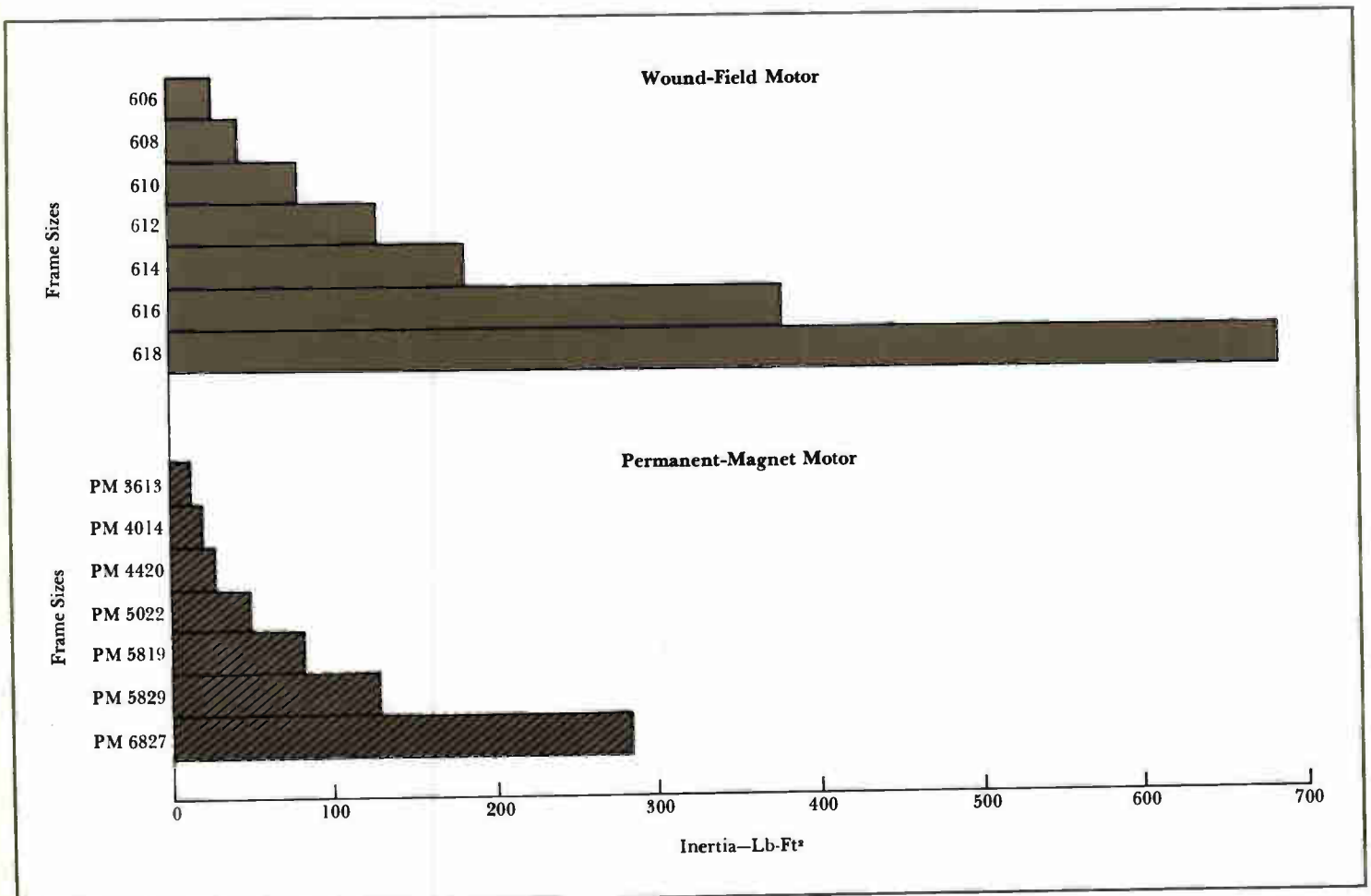

2—Armature inertia is much lower in permanent-magnet motors than in equivalent wound-field motors, providing faster speed response. The difference results from the higher main poles of the permanent-magnet motor and the consequent smaller armature diameter. The comparison here is between AISE 600 MC motors and equivalent Westinghouse permanent-magnet motors.

Calculating Motor Flux

A typical hysteresis curve for Alnico magnetic material is shown below. In motor design, only the demagnetizing portion of the curve (the second quadrant) is used; that portion and the saturation curves for the magnetic circuit in the motor are shown at bottom right.

The magnet is magnetized by applying a large magnetizing force to the excitation winding on the main poles, saturating the magnet to point *T*. When the force is removed, the flux follows the curve from point *T* to the intersection of the no-load saturation curve *NL1*, point *A*. The curves *NL1*, *FL3*, and *MX5* are the saturation curves for the flux through the magnetic main poles. The curves *NL2*, *FL4*, and *MX6* are the saturation curves for the actual useful flux passing across the airgap. When the motor is operating at the no-load point *A*, the no-load airgap flux is at point *B*. When a load is applied causing the demagnetizing curve *FL3*, the flux follows the curve to point *C* and the motor operates with an armature airgap flux point *D*. If the load is now removed, the flux follows a new minor hysteresis curve to point *I*. If points *A* and *I* are projected to the curve *NL2*, giving points *B* and *J*, the difference in flux between *B* and *J* is the no-load flux loss from no load to full load. When a maximum overload is applied causing the demagnetizing curve *MX5*, the flux follows the magnet curve to point *E*. If the load is removed, the flux follows a new hysteresis to point *K*. If point *K* is projected to the curve *NL2*, point *L*, the difference in flux between *B* and *L* is the loss in no-load flux from no load to maximum overload.

The loss in flux caused by the overload condition forces the motor to operate at a full-load flux point *N* instead of flux point *D*, resulting in the motor running faster. Any time the maximum overload condition exists, the loss in flux cannot be recovered until the magnet is fully magnetized by the excitation coils.

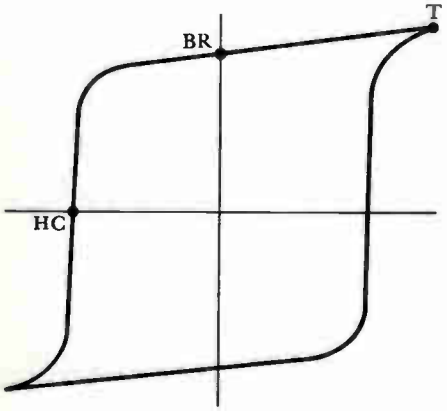

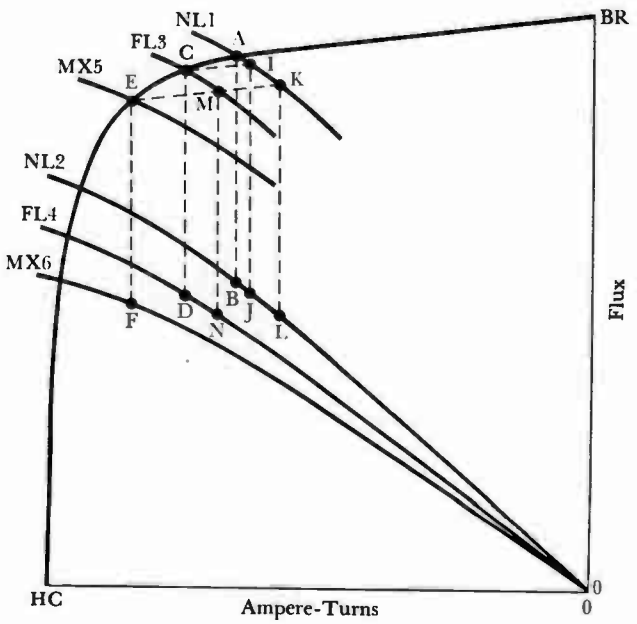

sign motors manually to meet customer specifications. It was a time-consuming task involving selection of parts from drawings and documents and then making detailed calculations to predict motor performance, so the manual method limited the number of designs an engineer could examine and seldom produced the optimum economical design.

Now, however, motor designs to meet customer specifications are selected by a computer program that gives the engineer the capability of examining a large number of designs before selecting the best one. The program logic is based on selection of a design that uses standard parts, so it gives the most economical design and helps reduce delivery time.

The computer program requires only a minimum amount of input information. The engineer specifies customer requirements such as horsepower, line volts, speed, and maximum overload condition on a simple input form (Fig. 3). The computer program selects a set of standard parts, calculates the performance of the motor, and compares that performance with customer specifications. If the design does not meet customer requirements, a new set of parts is selected from a table in the computer program, and performance is calculated and compared with specifications. Selecting, calculating, and comparing continue until a satisfactory design is found or the range of standard parts is exhausted. A satisfactory design using standard parts is usually found, but, if not, then special parts are used.

The computer output consists of the complete input, design limits, specifications, electrical parts selected, and detailed performance for each design (Fig. 4). The performance calculations predict operating speeds, torque, horsepower,

3—*(Top right)* The computer program used to design motors accurately to customer specifications requires only simple input. It selects parts that give desired rating and performance.

***Right*—Table roll drive, as in this steel mill, applies the permanent-magnet motor's advantages of low installation and operating costs, reliability, performance, and low maintenance requirements.**

JW001 IDENTIFICATION (ALL CARDS)

9 FOR LAST CARD

01	S.O. SAMPLE	G.O. BUFFALO	DATE- 12-10-68	ENGR- J. WACHOB	
02	H.P. 5.0	LINE VOLT 240.	BASE SPEED 1750.	DESIGN SPEC 1	ENCLOSURE DP

EXCEPTIONS

		CODE	DESCRIPTION	CODE	DESCRIPTION	CODE	DESCRIPTION	CODE	DESCRIPTION	CODE	DESCRIPTION	CODE	DESCRIPTION	CODE	DESCRIPTION
03	9	050	1450.	072	0.	100	256.01	101	256.01						
04															
05															

efficiency, commutating ability, and heat dissipating ability at various horsepower loads. From the computer output, the engineer selects the best design to meet customer requirements.

For economy, each frame size has one magnet, one pole design, and one airgap. To obtain the desired motor speed, the designer must vary the armature. (For a wound-field dc motor, not only can the armature be varied to obtain the desired speed but the flux level also can be varied by changing field coils and airgaps.)

All magnets used have been fully tested by the supplier to insure that they have the proper energy level. Testing coupled with an optimized magnetic circuit permits all the motors of a given design to approach ±2 percent of the average speed of the design, a very important feature for applications where the motors run in parallel.

More than 80 percent of the permanent-magnet motors shipped in the past five years operate on thyristor power supplies (TPS), and the permanent-magnet motor faces the same potential difficulties as wound-field motors in regard to additional heating and commutation problems.* Its construction gives the permanent-magnet motor a higher inherent inductance than equivalent wound-field motors; because of that increased inductance and because the permanent-magnet motor has no field-weakening speed range, commutation has not been a problem with permanent-magnet motors used on TPS.

However, ripple current peaks coming from a TPS can cause premature demagnetization. For example, a permanent-magnet motor may be overloaded to 900 percent of its totally enclosed nonventilated (TENV) rating with less than ½ percent loss in flux, while on a TPS the same motor may only be able to be overloaded to 750 percent before ½ percent loss in flux. The additional amount of flux the motor will lose on a TPS is difficult to calculate because the current ripple is a function of the total control and motor circuit, but tests have indicated that peak overloads must be reduced approximately 20 percent on semiconverter TPS and 10 percent on full-converter TPS.

An excitation coil, which is similar to a wound-field motor's shunt field coil, is used in a permanent-magnet motor to either magnetize or demagnetize the magnets. When the motor is assembled, the magnets are not energized because Alnico magnets lose most of their flux when not enclosed in a magnetic circuit. After the motor is assembled, the excitation coil is connected cumulatively to a dc power supply for two seconds to energize the magnets. The values of current and voltage required to fully energize the magnets is stamped on the motor's nameplate.

To dismantle the motor easily, the magnets should be demagnetized. The same coil is used again except now it is connected differential. The current value required to demagnetize the magnets (approximately ¼ of the current needed to energize them) and the corresponding voltage value are stamped on the motor's nameplate.

Advantages

Performance—The new permanent-magnet motor has approximately 10 to 15 percent more overload torque per ampere than does the equivalent TENV shunt-wound dc motor. In fact, the overload torque capability is very similar to that of a compound dc motor, with the torque output nearly linear to line current. The saturated design and the patented pole face design that keeps the loss in flux from overloads to a minimum are the main reasons for this high capability in overload torque per ampere.

The permanent-magnet motor has a flat speed regulation the same as shunt dc motors, but a major advantage of the Westinghouse permanent-magnet motors is that they are stable (no rise in speed with increase in load) out to maximum overloads for all sizes. The saturated design and the pole face design are the main reasons for the motor's stability. Standard shunt motors normally require series fields to be stable to full load on 75 hp and larger.

Since the flux produced by the magnet is not a function of temperature (below 300 degrees C), the only element in the permanent-magnet motor that varies with temperature is the armature circuit resistance. The change in armature circuit resistance from cold (just started) to operating temperature causes only a 1 to 2 percent change in the motor speed. Standard wound-field motors normally have a 15 to 20 percent change in speed from cold to operating temperature.

Reliability—With the elimination of the motor's field coil, the reliability of the motor is improved. And since field power is not required, field control components such as resistors, failure relays, and power supplies are not necessary; elimination of all those components greatly improves the total reliability of the system and reduces total maintenance requirements.

Installation Cost—When large numbers of motors are used, large savings can result from the elimination of field control hardware, field power supplies, and wiring; often, the elimination of control hardware alone offsets the additional cost of the permanent-magnet motor. Permanent-magnet motors have higher continuous TENV horsepower ratings than do equivalent wound-field motors, so for many duty-cycle applications they do not require external ventilation. That factor often amounts to substantial installation savings.

Efficiency—Permanent-magnet motors have 10 to 15 percent higher efficiency than equivalent wound-field motors. For battery operated applications, the result is longer service between battery charges; when large numbers of motors are used together, the higher efficiency cuts operating cost by a substantial amount.

Safety—Motor flux is produced by permanent magnets and, therefore, is independent of external power supplies. Permanent-magnet motors do not overspeed from an open field coil, since the

4—The computer output repeats the input and then gives the limits, specifications, parts selected, and calculated performance for the design. The engineer can have several design computations made and select the best one.

*V. E. Vrana, "The DC Motor and the Thyristor Power Supply," *Westinghouse ENGINEER*, July 1967, pp. 98-104.

PROGRAM ME2024 IDENT. JW001 S.O. SAMPLE G.O. BUFFALO DATE-12-10-68 ENGR-J WACHOB

FILE NO ME2008M REVISION DATE 68-10-25

HORSE POWER	= 5.00
LINE VOLTAGE	= 240.00
BASE RPM	= 1750
DESIGN SPEC	= 1
ENCLOSURE	= DP

EXCEPTIONS

50 = 1450. 72 = 0. 100 = 256.01 101 = 256.01

LIMITS AND SPECIFICATIONS

FIELD VOLTAGE	= 240.00
REGULATIONS	
SPEED(RPM)	= 1750.
MINIMUM(IN PERCENTS)	= 0.0
MAXIMUM(IN PERCENTS)	= 15.00
COMMUTATION	
SPEED(RPM)	= 1750.
PERCENT F.L. CURRENT(RPMB)	= 100.0
MAX. AVER. REACTANCE VOLTAGE	= 13.00
STABILITY	
SPEED(RPM)	= 1750.
PERCENT FULL LOAD	= 125.0
LOAD CAPACITY	
SPEED(RPM)	= 1750.
PERCENT FULL LOAD	= 115.0
MAXIMUM A FACTOR	= 1450.
MAXIMUM B FACTOR	= 10000.
TIME RATING	= 24.00
INSULATION CLASS	= 2.
DEGREES C (RESISTANCE)	= 95.0
MAX. ARMATURE TEMP. RISE	= 60.0
MINIMUM FRAME	= E256A
MAXIMUM FRAME	= E256A

(HP)B	(RPM)B	VL	VF	DESIGN	ENCL.	K	RA
5.00	1750.	240.00	0.0	1	DP	721.50	0.68210
	DAG	2BT/C	TYPE WDG	(RT)A	TARGET FL	SLOTS	RCUM
	0.12500	346.5	1	0.95500	91.00	25.	0.27290
		ARM ASSY	ARM PCHG	POLE PCHG	BR HOLDER	B T C	TPC C
	FR.2805A		2988439H01	870A025H03	4110065G060	99/ 3.50/2	55.0

	A	B	A*B	EBAR	E/IN	ECAVE
LIMIT	1450.	10000.	0.212E 07	28.00	400.0	13.00
CALC.	177.	3471.	0.616E 06	14.91	110.5	1.16

	EBR	DENBR	(AT)B	(FL)B	VENTS	ARM LG	ARM D
LIMIT	36.00	70.000	4600.	91.15	0/0.0	4.750	5.500
CALC.	4.29	17.701			4.750	4.750	5.500

L1	L2	L3	L4	LT	AREA M	LG M	CURVE
32.06	6.30	41.04	1.43	80.83	9.50	4.50	1

PERFORMANCE RPM = 1782. IL = 17.701 REG = 7.0

F.L.LOSSES HE = 53. PF = 4. EC = 0.0 FW = 43. FN = 0.0
BF = 39. SR = 299. SM = 0.0 BR = 35. SL = 42.

	NL	.5*FL	FL	1.5*FL	2.0*FL	MX	PT. L	PT. N
IA	0.64	8.85	17.70	26.55	35.40	144.61	0.65	17.70
IL	0.64	8.85	17.70	26.55	35.40	144.61	0.65	17.70
FLUX	89.79	99.73	89.50	89.51	89.01	81.73	89.50	89.22
RPM	1907.	1846.	1782.	1714.	1655.	882.	1914.	1788.
HP	0.0	2.50	5.00	7.31	9.41	18.84	0.0	5.00
TQ	0.0	7.11	14.74	22.38	29.85	112.13	0.0	14.69
EFF	0.0	87.7	87.9	85.5	82.6	40.5	0.0	87.9
LOSSES	157.4	260.3	515.7	920.8	1476.1	20655.8	157.7	516.0

NO LOAD SATURATION CURVE (MAXIMUM NO LOAD FLUX = 89.75)

flux from the magnet is always present. Also, dynamic braking can easily be added so that the motor can be stopped when the external power supply is entirely lost.

Two-Wire Systems—Many drive systems such as those on cranes have always used series dc motors to eliminate the need for a third wire. For most applications, however, a flat speed-torque characteristic is desirable, and permanent-magnet motors provide that characteristic.

Low Inertia—The low inertia of the Westinghouse permanent-magnet motor armature permits quick response.

Disadvantages

No Field Weakening—Permanent-magnet motors only operate at one field strength; they cannot be used when speed change by field weakening is required.

Cost—A given rating in a permanent-magnet motor normally costs more than the same rating in a wound-field motor because of the cost of Alnico magnets. (Very little is saved by the elimination of the field coil, since permanent-magnet motors have excitation coils.) For many applications, however, the reduction of installation cost due to elimination of field power and control may offset the higher cost of the motor and actually result in a lower total cost.

Demagnetization—As noted earlier, a permanent-magnet motor loses flux when overloaded beyond its design capability. Each frame size has a maximum overload torque it can produce before there is any loss in flux. That peak torque does not vary with the type of ventilation of the motor; it is a function of the sizing of the permanent magnets and the commutation ability of the motor. For continuous-nonventilated-rated motors, peak torque is in the range of 5 to 10 times the continuous torque. For one-hour-rated motors and continuous-force-ventilated motors, peak torque is in the range of 2½ to 3½ times the rated torque. When thyristor power supplies are used, current ripple causes an additional reduction of the motor's maximum overload torque. Demagnetization from overloads is not normally a problem for a continuous-nonventilated-rated motor. With either short-time-rated or force-ventilated permanent-magnet motors, especially when used with a TPS, the maximum overload torque the motor must produce without demagnetization is often what sizes it.

Unfortunately, there are a few applications that abuse dc motors to the point where flashovers are common. For those applications, demagnetization can be a problem and therefore permanent-magnet motors are not recommended.

Applications

Although the permanent-magnet motor was originally designed for the steel industry, it is now commonly used in practically all industries. Seldom are permanent-magnet motors used just to eliminate the field coils and excitation; they are used when their advantages provide the user with economy and superior performance.

Cost difference between small permanent-magnet motors and small wound-field motors is slight, while the difference for larger motors is considerable. The reason is that the larger motors require larger proportional pounds of magnet compared to the total pounds of the motor (to keep from losing flux during overloads) than do the smaller motors. The magnet cost of the larger permanent-magnet motors may be as high as half the total cost of the motor. It is this higher cost of the larger permanent-magnet motors that has limited the number of them applied.

The largest size built to date by Westinghouse is 400 hp. It is being used to drive an ingot buggy in a steel mill; the additional cost was justified by savings in installation and operation cost and by improved safety.

Following is a general classification of applications in which permanent-magnet motors have been applied:

Large-Quantity Applications—The table roll drive is an example of this type. Each motor usually drives a single roll, with as many as a thousand motors used in one installation. The advantages are lowest first cost for the total system, lowest operating cost, improved overall reliability, reduced maintenance, and improved motor performance.

Duty Cycles—In many applications such as screwdowns, loopers, arc-furnace drives, and press-feed drives, the motor is required to work at full field continuously while the average torque output produced is very low. Since a permanent-magnet motor is always operated at full field without any field heating, the low average torque output required of the motor, coupled with a higher continuous TENV capability, allows use of a smaller motor, enclosed frame instead of open frame, or complete elimination of external cooling.

Many of these applications have a motor driving the load through a large gear reducer. Often the reflected inertia from the load back through the gear reducer is small compared to the motor's inertia, so the motor's inertia is the major load during acceleration. Since a Westinghouse permanent-magnet motor normally has half the inertia of the wound-field motor, it therefore has faster response and outperforms the wound-field motor.

Battery-Operated Traction—Permanent-magnet motors are used as traction motors on vehicles that have the gear ratio set for maximum load at top speed (e.g., personnel carriers and mine tractors). The high efficiency gives 15 to 20 percent longer battery life between charges. Additional advantages are high overload torque per ampere, flat speed regulation that keeps the vehicle from overspeeding, and ease of dynamic braking. Moreover, permanent-magnet motors can regenerate power to the battery.

Two-Wire Systems—Because of their flat speed-torque characteristic, many permanent-magnet motors are being used in place of series motors for such two-wire applications as cranes, coil tong drives, and hydraulic pumps.

Conclusion

Many thousands of permanent-magnet motors have been built and used in varied applications. Although most have been used in the steel industry, the number of other applications will continue to increase as industry becomes aware of the motors' unique characteristics.

Control Computer Can Ease Process Startup

G. S. Rambo
Vester S. Buxton

Imaginative use of the process control computer while the process is being installed and started up can reduce the time and expense required for startup far below what has been considered normal. An example is the recent startup of the new Armco hot strip mill.

Although digital process control computers are purchased primarily for their long-term benefits in *operating* the process, using them to help *start up* the process can yield significant additional savings. That capability was demonstrated recently at Armco Steel Corporation's new hot strip mill at Middletown, Ohio, where startup and production were accomplished in a smoother manner and shorter time than could normally be expected, resulting in savings of millions of dollars in break-in costs. The manner in which the process control computers were integrated into, and utilized in, the overall startup plan was a major factor in the startup.

Using the computer to verify and calibrate the operation of the many subsystems to which it is connected is, then, an extremely useful and powerful tool during startup. However, it requires adequate planning and scheduling and a computer hardware and software package whose factory and on-site operation has been proved by combination testing.

Total Planning

The first step in applying a computer control system is to analyze the *total* job, with particular emphasis on the computer —the piece of equipment that will eventually manipulate almost all of the conventional equipment purchased. When the purchase of the computer is made on a sound economic basis and with all personnel understanding its short- and long-term benefits, the system can enable the user to reach levels of quality operation unobtainable only a few years ago.

Initially, the user must plan a coordinated functional system and win unequivocal commitment to that system from all departments, especially the operating portions of the organization. Then operating personnel must be thoroughly trained in the use of the computer.

Operator acceptance can be enhanced during installation by a common-sense approach. For example, the computer should always be installed and started up simultaneously with the more conventional controls. Then a few problems with the computer are not highlighted and overemphasized, because every part of the system has its problems during shakedown. In such an environment, the operator gains confidence in the computer (or, more correctly, does not lose confidence). The successes of the computer are a part of those of all the control equipment, so the operator tends to treat the computer as just another of his tools.

Full production demands on the process should be deferred for a time to allow all contributing parties to experiment with and tune the control system. Such an approach permits greater familiarization with the operating system and its capabilities—a prerequisite to optimum performance.

The Armco startup plan included a detailed "line-of-balance" schedule that showed the interfaces between control elements, electrical drives, wiring, and construction. The startup schedule was coordinated with Armco and each separate activity tied to a key event. Since the coordinated schedule allowed the progress of each activity to be measured relative to every other activity, all control elements were available when needed. Thus, as each event was reached, the proper resources were there to accomplish the next activity.

Startup moved smoothly, and even delays did not disturb the pattern. As a result, the first attempts to roll steel in the roughing mill were successful, as were the first attempts to roll from one end of the mill to the other.

Computer in Startup

Among the many advantages that can be gained by intelligent and imaginative use of the computer during startup, a prime example is tuning a rolling mill's po-

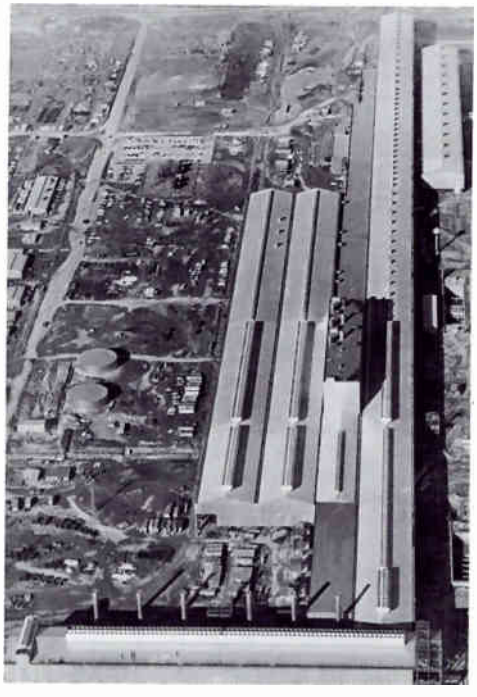

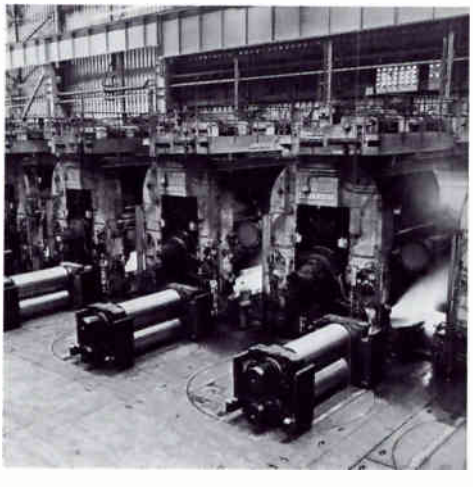

***Top*—Hot rolling complex at Armco Steel Corporation, Middletown, Ohio, includes the most automated hot strip mill in the world, with five computers to control it from start to finish. The shorter leg of the "L" houses soaking pits where ingots are heated; the steel then goes through a slab mill and roughing and finishing mills. The mill was started up with the aid of its control computers.**

***Bottom*—Finishing train at the Armco mill reduces incoming steel bars to thin strip. The mill operates on full computer control, although operators can assume manual control when desired. The automatic roll changers beside the mill stands change work rolls quickly when they become worn.**

G. S. Rambo is Manager, Metals and Process Systems, Hagan/Computer Systems Division, Westinghouse Electric Corporation, Pittsburgh, Pennsylvania. Vester S. Buxton is Industrial Sales Manager at Hagan/Computer Systems Division.

sitioning subsystem to compensate for friction and other mechanical restrictions. Rolling requires accurate positioning of screwdowns (for thickness reduction), edgers (for width control), and sideguards (for control of material position on the tables). The position regulating system in a Prodac 50 process control computer has a self-tuning feature that allows the computer to run the positioning drives at top speed and then stop them under maximum braking torque (current limit) at the exact point desired without overshooting or creeping.

By observing the time it takes to traverse a specific distance for a particular control voltage, the computer automatically constructs a slowdown table that establishes the relationship between distance from target and drive speed for each positioning drive. Knowing the length of travel remaining, the computer determines the maximum operating speed for each point that yields a no-overshoot stop at the target reference. The positioning drives are then controlled in accordance with the slowdown tables for optimum response and accuracy.

An adaptive positioning control feature (not on the Armco mill) has been used to optimize positioning performance of other mills, where operation of the electrical-mechanical positioning system is not consistently predictable. With adaptive control, the computer continually observes actual performance. If the stopping

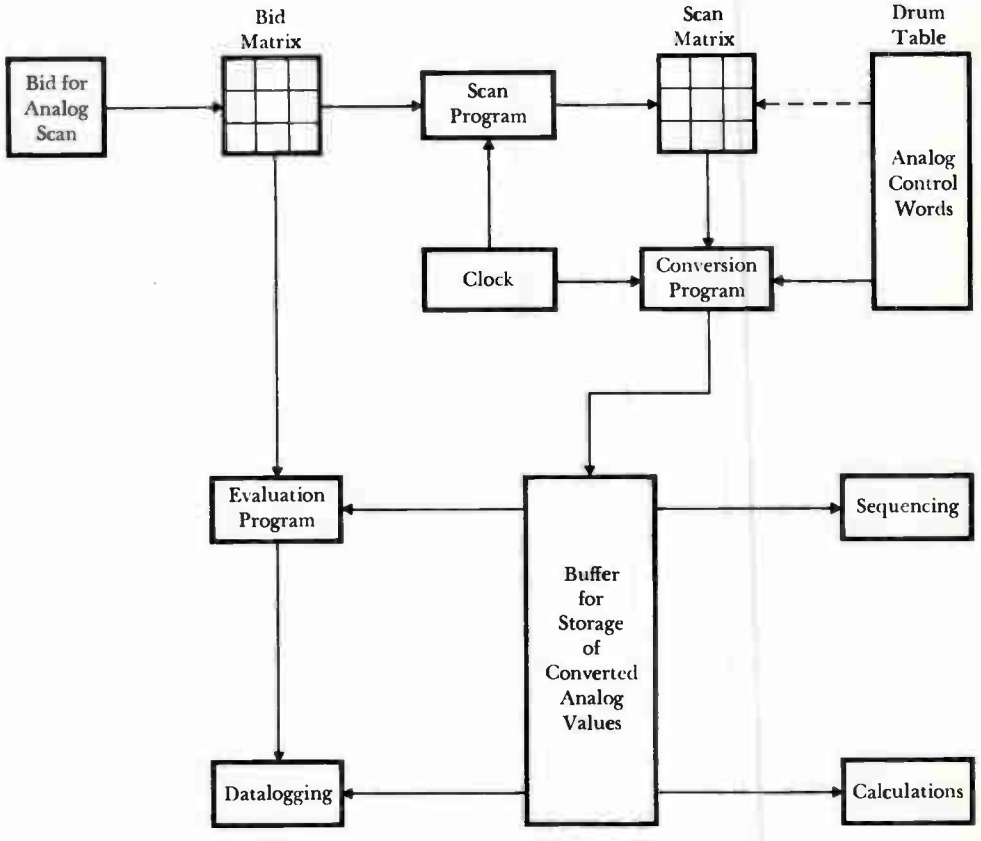

1—Information flow in the analog programs of a process control computer. Such programs can be used by the computer before process startup to verify and calibrate the process's electrical subsystems.

2—The Armco hot strip mill is represented here in greatly simplified form. It was started up one area at a time, beginning with the roughing mill, after the subsystems had been verified.

characteristics change, due to friction changes for example, the computer automatically corrects its slowdown table to compensate for the changes in the electrical-mechanical system.

Other electrical subsystems can also be calibrated and verified by the computer through the analog programs. An example is calibration of the temperature sensors in a furnace. The computer first checks polarity by reading the voltage at an analog input. Since negative temperature is not valid, a wiring error can thereby be discovered. Next, the computer converts the analog input voltage to temperature by the manufacturer's recommended conversion technique, giving a value in engineering units for the temperature being measured by the sensor. It is then a simple matter, by using alternate sensor systems, to adjust the sensor to provide the proper voltage level in accordance with the computer's analysis.

Operation of the analog input program is diagrammed in Fig. 1. The scan program is initiated at predetermined intervals (controlled by the computer clock), with the drum table correlating selection of the inputs that represent the desired variables. The conversion program translates the voltage received into proper engineering units and stores it in the buffer until the data is used for evaluation or logging purposes. The data in the buffer is available to all control programs in the software system. Because closed-loop control depends on the feedback values, use of the computer program to calibrate sensors initially assists the overall startup.

Another example is calibration of the subsystem that controls the speed of the motor-driven tables used to move steel from one point in the process to another. As the steel passes through a mill stand, entry speed is less than exit speed because thickness is being reduced and mass flow must be constant. (The condition is similar to that of fluid flowing through a constriction in a pipe.) Therefore, entry table speed must be "draft-compensated" by an amount depending on the draft (amount of reduction) taken. The computer controls speed by setting a reference to the table. During startup, the computer can be used to observe speed feedbacks and indicate deviations from speed reference settings. The information can then be used to calibrate the draft-compensation settings.

Moreover, the computer can read and log the results of thousands of inputs to verify operation of thumbwheels, pushbuttons, pushlights, displays, and other contact communication devices.

Thus, effective use of the computer as a central information point can measurably reduce the time necessary to pinpoint errors in auxiliary control subsystems. The computer acts as a central debugging device for verifying the operation of all connected system components.

After the subsystems have been verified, the mill startup is approached functionally by processing areas. At Armco, the first area started was the roughing mill (Fig. 2). Programs were included in the computer to simulate the actual presence of steel, and the total control system was checked in this dry-run mode. Thus, the computer verified the operation of all main roughing-mill systems without endangering any mill equipment.

Conclusion

The decision to purchase process control computers will continue to be made on the basis of long-term benefits. However, computers have proved that their effective use in putting a major process on line can yield important additional economic benefits. Conversely, lack of proper planning for their use can result in unnecessary delays for the user and cost overrun for the computer supplier.

The Armco installation is one of several hot strip mill applications where initial operation was sufficiently satisfactory to permit reduction of pilot operation time in favor of starting production. Two slab mills, a variety of process lines, and several steel-making facilities have also demonstrated the validity of this installation approach. Less realistic approaches too often result in dissatisfaction without a clear understanding of the reason for failure to achieve the desired goals.

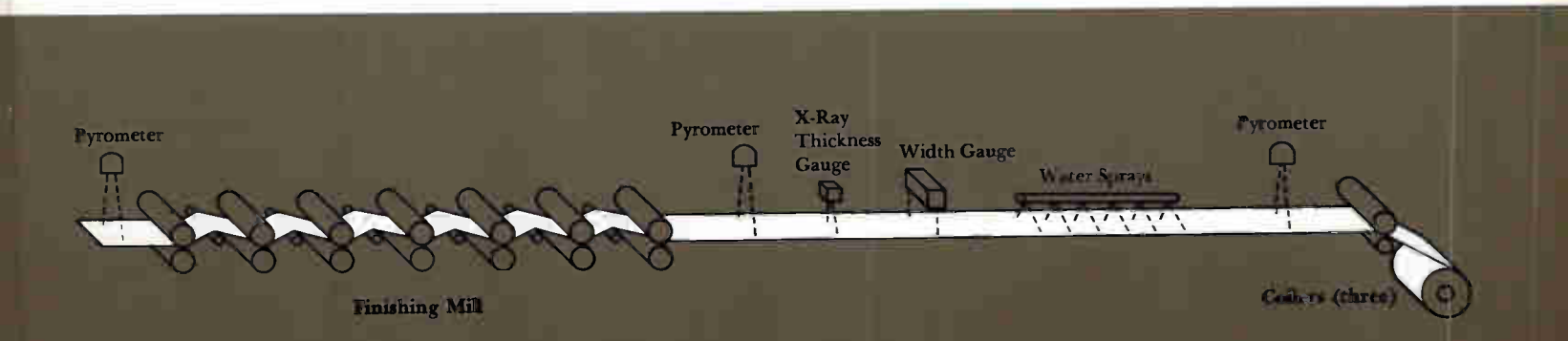

Fundamentals of Pulse Doppler Radar

L. P. Goetz

Pulse doppler radars provide the search and track functions for today's aircraft and missile systems. Use of the doppler effect separates moving targets from regions of high background clutter.

Modern doppler radars, particularly those used in today's high-speed aircraft and missile systems, have advanced several technological generations from the first doppler radars that were developed during World War II. Those early versions were ground-based radars, designed to avoid the great amount of ground clutter (reflection from land or sea surface) that results when ground or ship radars search the sky at low elevations to pick up distant aircraft. By utilizing the doppler effect, radar reflection from an oncoming aircraft is shifted sufficiently in frequency to permit the radar receiver to receive the target return signal at frequencies removed from the ground clutter return.

Today's radars for high-speed aircraft and missiles also use the doppler effect to separate moving target returns from regions of high background clutter. However, missile and aircraft applications require one major design innovation from the earlier versions of doppler radar. Since transmitting and receiving antennas cannot be physically separated far enough to provide the necessary signal isolation between transmitter and receiver, it is necessary to alternate the transmit and receive cycles. Radars of this class use a single antenna, time-shared between transmitter and receiver, so they are called *pulse doppler radars*.

A typical pulse doppler application for missiles is the final guidance phase of target acquisition. For example, a ground-based interceptor missile is guided from ground to the target's vicinity and elevation, where the pulse doppler radar is then activated for the terminal guidance phase. The high relative speed between missile and target provides sufficient doppler shift to separate the target return from background clutter.

In aircraft applications, a typical pulse doppler radar is used in a *search* mode to hunt for moving targets. Upon target acquisition, the radar switches to a *track* mode to guide the aircraft to the target.

L. P. Goetz is a staff engineer with the Radar Systems Group, Aerospace Division, Westinghouse Defense and Space Center, Baltimore, Maryland.

Doppler Shift

Doppler radars operate by detecting the doppler shift introduced by a target that has a radial velocity component with respect to the radar. All modern doppler radars detect the amount of frequency shift rather than the actual frequency of the return signal. The equation for doppler shift can be written:

$$f_d = \frac{103\ V}{\lambda}$$

where f_d is the frequency shift in hertz, V is the radial velocity of the target (relative to the receiver) in knots, and λ is the operating wavelength of the radar in centimeters. Thus, for a doppler radar operating in the three centimeter wavelength region (X band), the doppler shift is about 34 hertz per knot of relative radial velocity.

A typical pulse doppler transmission is the pulsed carrier wave shown in Fig. 1. The carrier wavelength is usually in the centimeter range (3-30 GHz). From the doppler equation, it can be seen that the frequency shift produced by a typical moving target is relatively small compared with the carrier frequency. For example, if a Mach 2 aircraft and a Mach 2 target are closing on each other, the closing velocity is about 2700 knots. At 34 hertz per knot, the doppler shift is only 92 kHz. Thus, to accurately separate the doppler frequency from the high carrier frequency, extremely stable transmitter and receiver oscillators are required. Typically, a stable reference source is used for radio frequency generation, and a fixed offset from this frequency is used to determine the amount of doppler shift. This technique simplifies the stable oscillator design, and the tolerable short term stability.

Pulse repetition rate—The minimum pulse repetition frequency (PRF) is set by the anticipated doppler frequency. One criterion for selecting PRF is Nyquist's sampling theorem, which specifies that a necessary condition for reconstructing a wave form is that the sampling frequency be at least twice the frequency of the wave form being sampled so that the information will not be ambiguous. For the example given, PRF must be at least twice the maximum anticipated doppler frequency (92 kHz), or about 200 kHz.

Frequency Spectrum of Pulse Doppler Signals

A transmitted carrier chopped at a continuous PRF can be shown by Fourier analysis to consist of frequency components that form a grouping of spectral lines about the carrier frequency. The interrelationships between carrier frequency (f_0), pulse repetition period ($T = 1/PRF$), and pulse period (τ) for a chopped carrier are shown in Fig. 2.

The spectrum of the returned signal is essentially the same as the transmitted signal except that each spectral line is shifted by the amount of the doppler frequency (f_d). The magnitude of the doppler shift is the measure of relative velocity between radar set and target. If this shift could be measured directly, it would provide within itself all the information on the target measurable on a frequency basis. However, since it is not practical to measure doppler shift directly, the received signal is heterodyned to an intermediate frequency and detection then removes the intermediate frequency component to provide a detected frequency spectrum (Fig. 3) from which the desired doppler information can be derived.

Since the desired doppler information is contained in the frequency distribution associated with each PRF spectral line, signal filtering limits the bandwidth actually selected for detection to a portion of the spectrum associated with a single spectral line. Signal heterodyning produces a doppler signal both above and below each PRF spectral line (i.e., $f_0 + f_d$ and $f_0 - f_d$), so doppler shift (f_d) must not be allowed to exceed one half the PRF or the doppler signals from adjacent PRF spectral lines will overlap, making it impossible to resolve doppler frequency. Thus, the maximum doppler shift that can be detected unambiguously is limited by the PRF, $f_{d_{max}} \geq PRF/2$.

This, in effect, is the pulse doppler

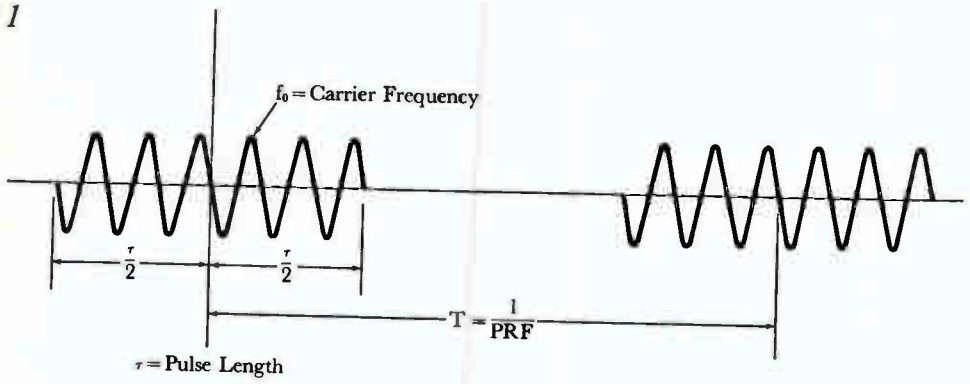

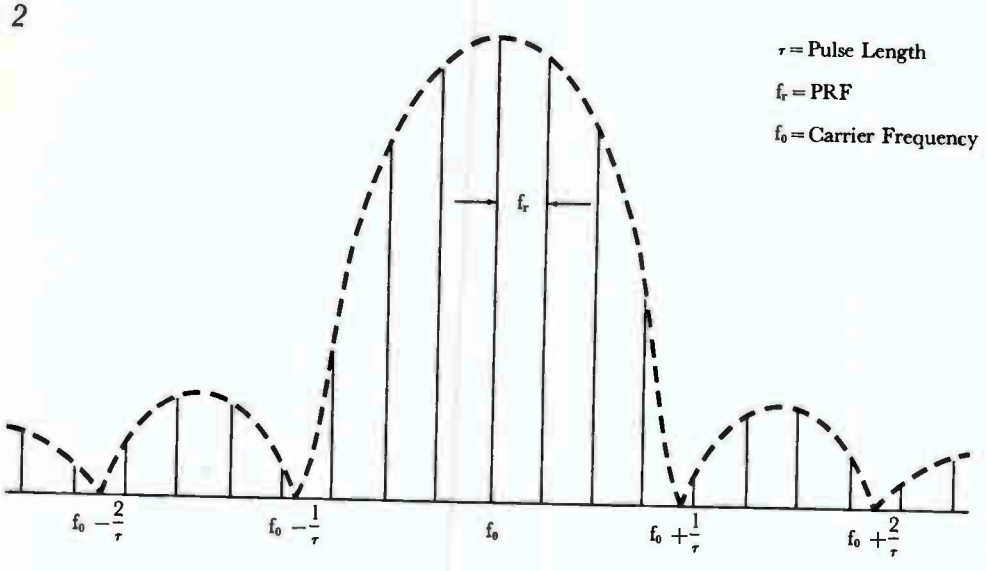

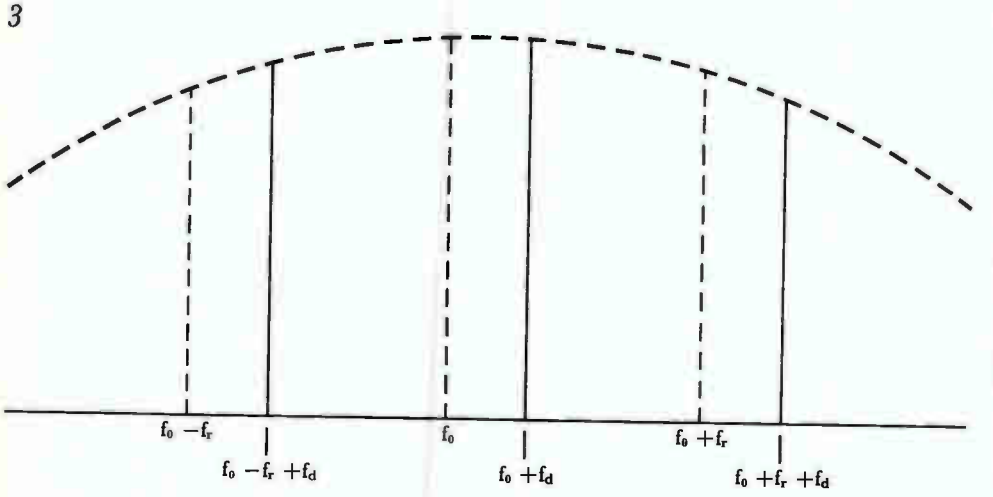

version of the application of the Nyquist sampling theorem.

Clutter Spectrum

Clutter in a radar set is the reflection of nontarget objects from either the main beam or the antenna side lobes. In aircraft pulse doppler radar, clutter originates from the three sources illustrated in Fig. 4. Main beam clutter is the backscatter from ground when the main beam dips below the horizon; it is relatively strong because of the strength of the main beam. Side-lobe clutter comes from the antenna side lobes striking the ground at various angles, and it produces doppler shifts both above and below the transmitted carrier frequency. Side-lobe clutter has a range of doppler frequencies corresponding to twice the ground velocity of the aircraft. At any particular instant, one of the side lobes is looking straight down at the earth and returns a signal with zero doppler shift. This altitude line occurs in all airborne radars.

The distribution of the clutter spectrum about each spectral line in the return signal is shown in Fig. 5. Depending on the size of the nontarget object, its bearing, and its relative velocity and range, its reflection may obscure a desired target. The basic problem is to arrange the parameters of the radar set such that clutter is minimized in the frequency region where targets are expected. Thus, to appear in a clutter-free region, an approaching target must have a closing velocity such that its doppler shift is greater than the closing clutter to the right of the spectral lines in Fig. 5. However, closing velocity cannot be too great or its doppler shift will run into the open-

1—Pulse doppler transmission is a pulsed sine wave.

2—Frequency spectrum for pulsed sine wave is a grouping of spectral lines above and below carrier frequency (f_0) encompassed by an envelope whose shape is determined by the shape of the transmitted pulse.

3—Spectral lines of detected signal spectrum are shifted above or below return signal spectral positions by doppler frequency (f_d), depending on whether the target has a closing or opening velocity.

ing clutter of the neighboring spectral line. Since the spectral lines are separated in frequency in direct proportion to the PRF, the PRF determines the range of closing target velocities that can be handled unambiguously by the radar. The range of opening target velocities that can be detected is similarly limited.

The effect of each of the various types of clutter for different target headings is shown in Fig. 6. An aircraft with a scanning antenna is flying in the direction shown. Two targets are indicated, one directly ahead of the aircraft and one at an azimuth angle of 45 degrees. Each target is located at the center of circles that represent ratios of target ground velocity to interceptor ground velocity. A target vector showing velocity ratio and direction is drawn from the center of each target position. The tip of the vector shows whether the target is clear or obscured by clutter.

The two target vectors illustrated in Fig. 6 show the targets to be outside the clutter region. If both targets were traveling opposite to the directions indicated, the target straight ahead would be obscured by opening side-lobe clutter, but the target on the 45-degree bearing would be clear of opening clutter because of its higher velocity.

4

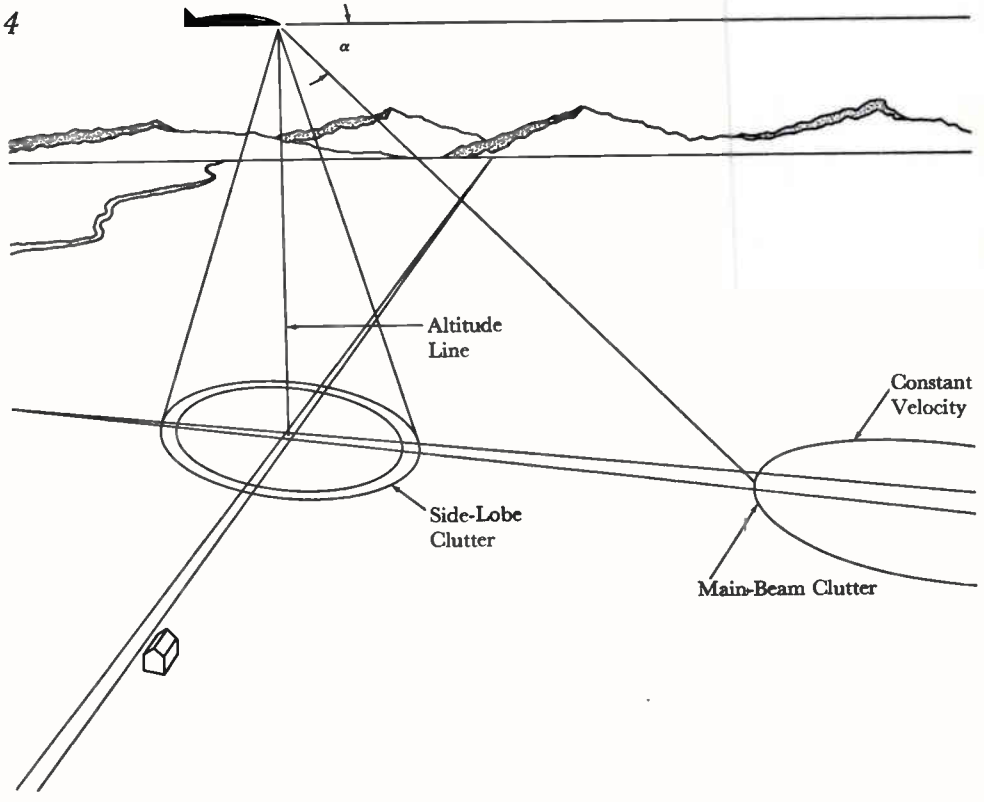

Range Resolution

In pulse doppler radar, as in conventional pulsed radar, range to the target is proportional to the time interval between a transmitted pulse and its return echo. However, the high pulse repetition frequency that must be employed with pulse doppler radars causes many time-around echos and corresponding ambiguities in range information.

Several techniques can be used to resolve such ambiguities. One typical ranging system uses multiple PRFs. The principle of the multiple-PRF system can be described by considering the two-PRF system, illustrated in Fig. 7. The basic ranging frequency sets the maximum unambiguous range that can be measured. Two higher frequencies are then derived from this basic frequency by multiplying by two integers. In the example shown, the integers are 3 and 4. Target returns

5

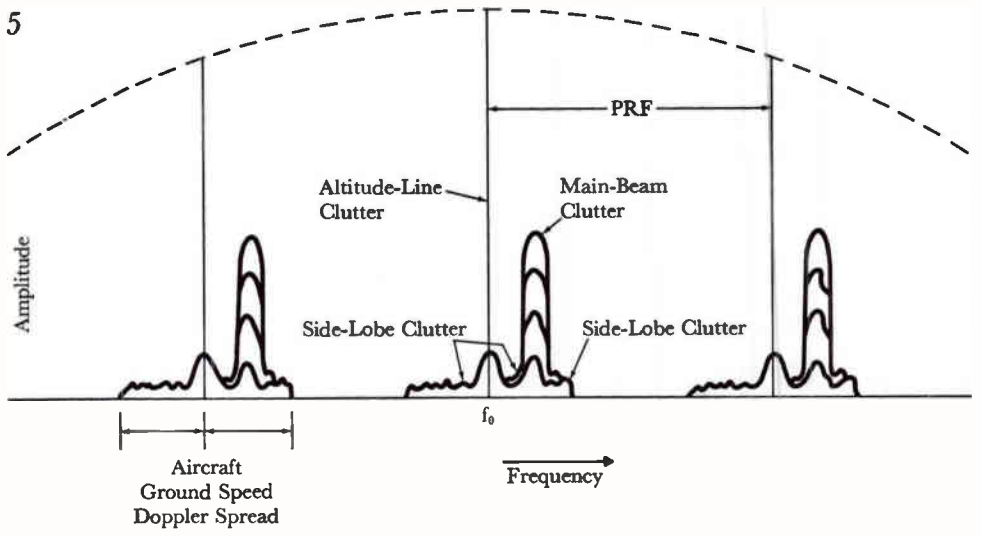

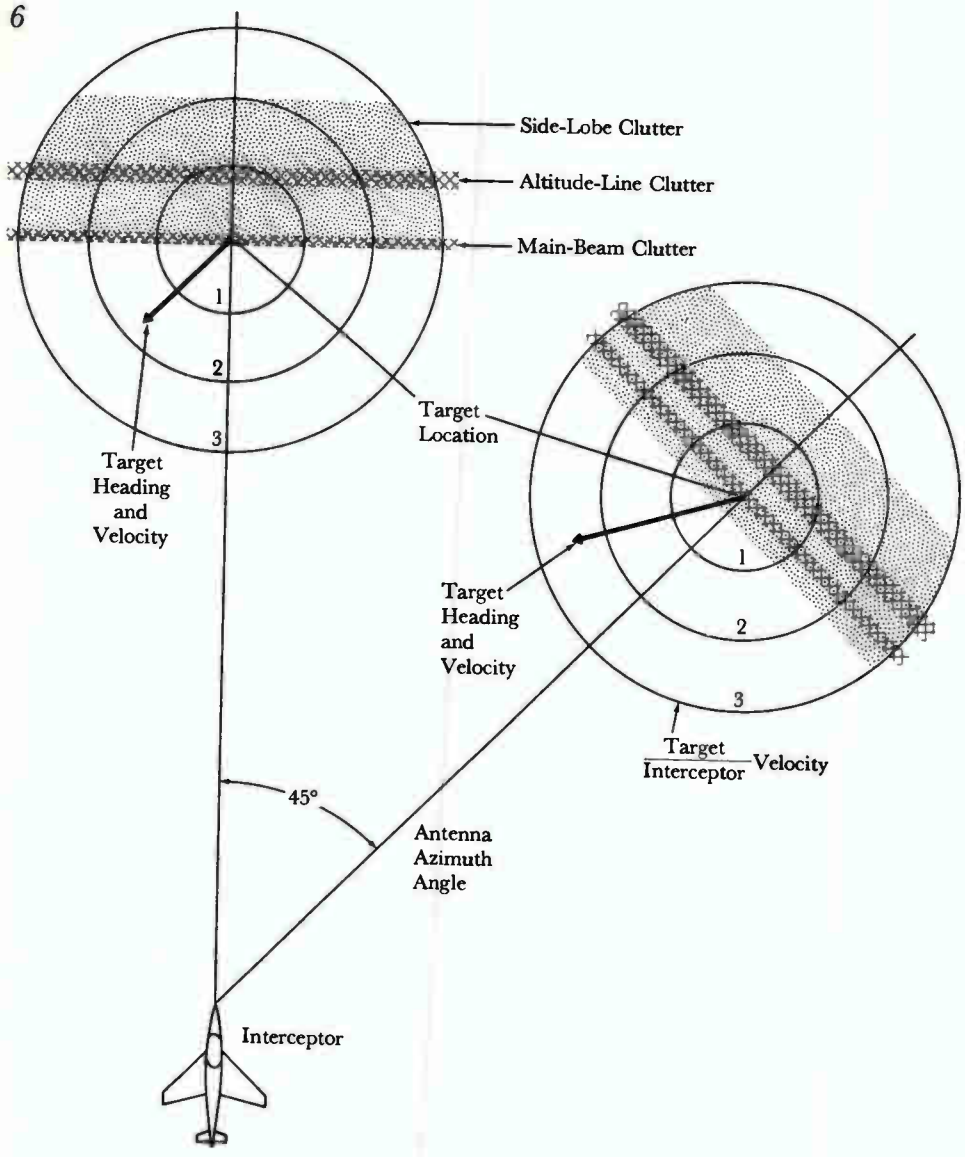

4—Clutter in an airborne pulse doppler radar is generated by reflections from main beam and side lobes.

5—Typical distribution of clutter around each spectral line in an airborne, nose-mounted pulse doppler radar.

6—Clutter and target vector diagram illustrates whether target will be clear or obscured by clutter.

produced by each of these PRFs are ambiguous, but these returns will coincide at the true target range. Thus the radar transmits alternately at each PRF, and stores the returns for comparison. Return coincidence gives true range.

This multiple-PRF technique can be extended to a number of PRFs, but, in practice, a two- or three-PRF system can usually resolve the range problem.

Target eclipsing—Range calculation for a pulse doppler radar is similar to the range calculation of other types of pulse radar with one exception, and that is eclipsing of the target reflection by the transmit cycle. Because many transmit pulses occur between the transmission of a particular pulse and the return of its echo, it is quite possible for all or part of the echo to return during a transmission pulse, causing the target to be "eclipsed." With reasonable antenna-scan speeds, the amount of eclipsing may not change appreciably during the dwell time of the antenna main beam on a target during a particular scan. However, when the antenna returns to the target on the next frame, the target will have moved to a new position where the eclipsing may be more or less than on the previous frame. Typical frame times are of the order of one second, so a Mach 2 target would move about 2000 feet between frames.

If the target velocity is such that it moves a distance corresponding to an integral number of interpulse periods during the frame time, the target may be eclipsed on all looks and range performance would be significantly degraded. To prevent such "blind" target speeds, the PRF can be changed in a periodic manner. This has the effect of averaging the eclipsing from frame to frame instead of from target to target. For example, with a single PRF, one target could be completely eclipsed while another target could be completely clear. Periodic changing of PRF would cause the eclipsed target to be alternately clear and eclipsed.

A representation of range performance for a pulse doppler radar can be developed for a target assumed to start at a range where the probability of detection is small and to move radially toward the radar at uniform speed (Fig. 8). A proba-

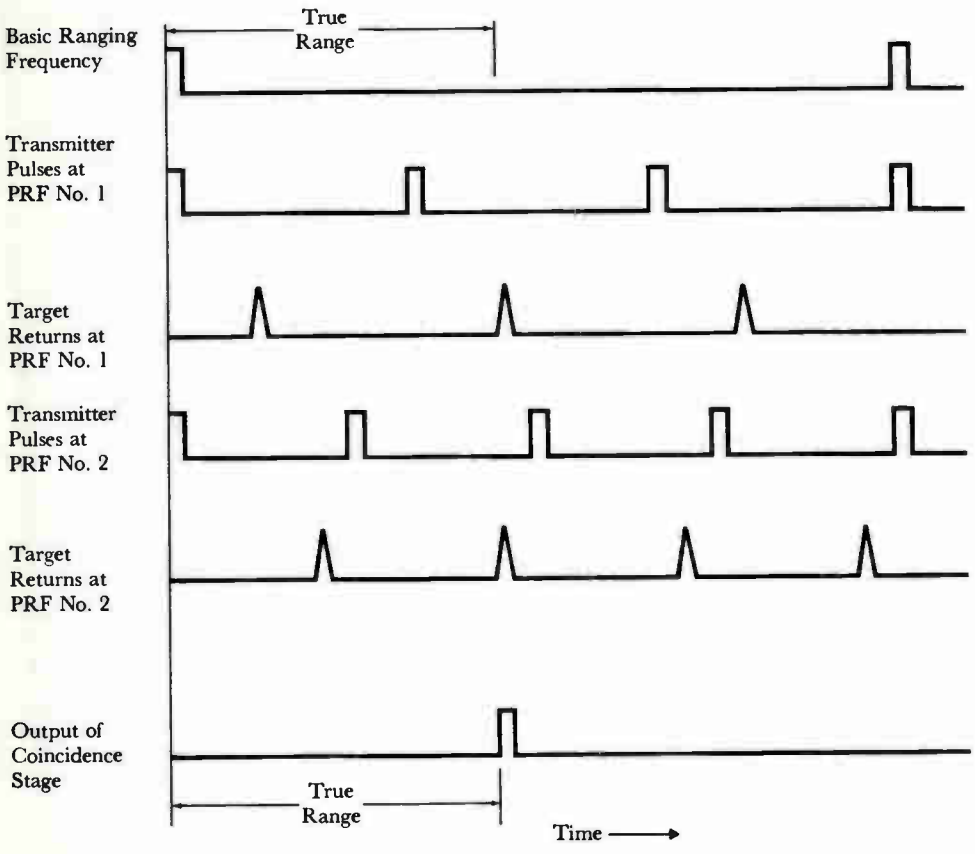

7—The target returns of a two-PRF ranging system coincide at true range only.

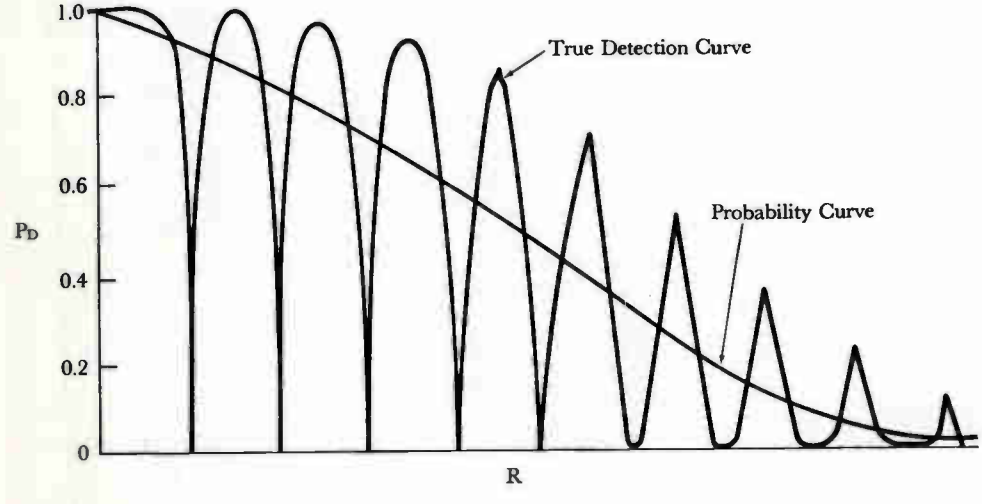

8—A smoothed detection curve that represents probability of target detection can be derived from true detection curve.

bility of detection curve is derived from the true detection curve for this situation, which is a series of loops with loop spacing determined by the PRF Thus, return signal strength varies from frame to frame, depending on frame time, relative velocity, PRF, pulse width, and range.

Elements of a Pulse Doppler Radar

A block diagram of a typical pulse doppler radar for aircraft application that will search for a target and track it in velocity, range, and angle is shown in Fig. 9.

In the *search* mode, the target is located in velocity and angle. The modulator keys the transmitter to produce a pulsed sine wave, and the return signal is routed to a mixer via an isolator. The mixer translates the received frequency to an appropriate intermediate frequency (i-f), which is amplified and passed through a band-pass filter. Filters for rejection of clutter may also be included at this point to provide additional clutter attenuation. Bandwidth is reduced as early as possible to simplify amplifier design by reducing dynamic range requirements.

The output of the band-limited i-f stage feeds another mixer which translates the frequency spectrum to one satisfactory for a contiguous filter bank that encompasses the target doppler frequency range of interest. (An analogy to a contiguous filter bank in the power frequency field is the vibrating reed frequency meter, in which a bank of resonant reeds is used to measure frequency.) The contiguous filter bank arrangement permits the radar to search the whole desired doppler frequency range simultaneously.

When a target is detected, the detection and decision unit switches the radar to the *track* mode. Antenna scanning is stopped, the velocity track loop is locked on target using information from the contiguous filter bank for velocity track positioning, range track is initiated, and angle track is started.

Techniques similar to those used in conventional pulse radar are satisfactory for range and angle track, and velocity track is performed with either a phase or frequency track loop. It is common practice to also feed velocity information to the range track feedback loops to aid in

target range tracking.

The precise signal generation and signal processing requirements of airborne pulse doppler radars are not easily satisfied. For example, the signal strength of a typical target return might be only 10 dB above thermal noise, whereas main beam clutter will be some 90 dB above thermal noise. Any spurious modulation of the transmitted carrier would have the effect of spreading the clutter spectrum and completely masking the target return. Thus, all spurious modulation of the carrier must be kept at least 80 dB down from the level of the transmitted carrier. This means that the carrier signal must approach a textbook sine wave, completely free from the influence of aircraft vibration, power supply ripple, or leakthrough from any other part of the system. Furthermore, the carrier frequency must be completely free from short-term drift.

9—Diagram of typical pulse doppler radar that searches for and tracks moving targets.

These high performance requirements have required continual advancements in the technology: oscillators that are extremely accurate and free from the effects of aircraft or missile vibration, filters that can remove or select frequency bandwidths with high precision, and components that can withstand the difficult airborne environment with high stability and reliability. In fact, the technology that existed only 20 years ago would simply not have permitted the development of today's operational pulse doppler systems.

Systems for the Future

In multipurpose airborne radar systems, pulse doppler is often just one of several possible required modes of operation. For example, the total radar system may also provide a pulse mode, a chirp mode, and a mapping mode. Each mode requires a specific combination of transmitted signal and return signal processing.

One of the more promising techniques now being demonstrated for the next generation of multimode airborne radar is digital signal processing. With digital techniques, signal processing is accomplished with programmed instructions rather than with specific arrangements of circuitry required for analog signal processing. The operation of multimode systems would be simplified because changes from one mode to another could be accomplished merely by changing programs rather than hardware.

Digital signal processing in the radar frequency range requires extremely high data rates. These high rates are now feasible with high-frequency molecular circuits that are small, lightweight, and reliable. In addition to simplifying operational techniques, digital signal processing also offers the potential of radar systems that are smaller, lighter, and more flexible than today's analog designs.

REFERENCE:
Goetz, L. P. and Albright, J. D., "Airborne Pulse-Doppler Radar," *IRE Transactions on Military Electronics*, Vol. MIL-5, No. 2, April 1961, pp. 116-126.

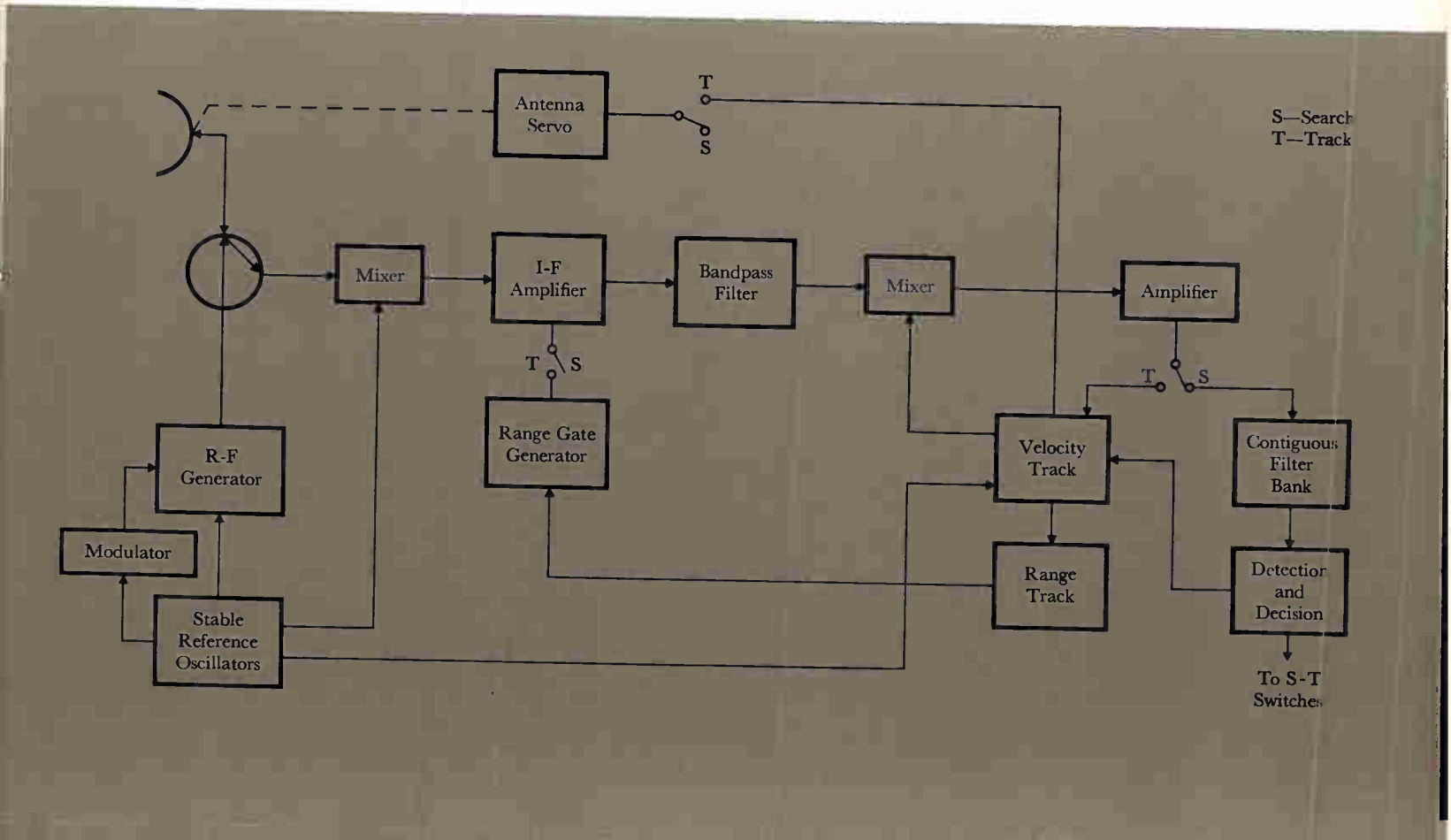

Technology in Progress

Silicon Carbide Rectifiers Can Operate at 500 Degrees C

Silicon carbide rectifiers have been developed that can operate at more than double the temperature it takes to disable silicon rectifiers: they can function at 500 degrees C and survive temperatures of over 980 degrees C. In contrast, silicon rectifiers are limited to temperatures below 200 degrees C, because at higher temperatures they become metal-like and conduct current in both directions.

Silicon carbide rectifiers with forward currents up to 10 amperes and reverse voltages to 300 volts have been produced. The new devices were developed by the Westinghouse Astronuclear Laboratory from research work done there and at the Westinghouse Research Laboratories. In addition to their higher operating temperature, silicon carbide rectifiers are inert in most atmospheres and are highly resistant to ionizing radiation; preliminary results show resistance to radiation damage at least ten times that of comparable silicon devices.

Junctions are produced in the silicon carbide crystals by adding suitable impurities—p-type and n-type dopants—to form a layered structure. Machining techniques (mechanical and chemical) for the crystals are similar to those used for silicon. However, mechanical machining such as lapping, abrasive cutting, and ultrasonic cutting must be done with diamond or boron-carbide dust because those are the only materials harder than silicon carbide.

Chemical machining requires radical departures. Etching, for example, requires great care because hexagonal silicon carbide is a structurally polarized crystal with a carbon face and a silicon face; etching rates on the carbon face are usually much faster than those of the same etchant on the silicon face. Moreover, the etchants themselves can be problems because of their reactivity with silicon carbide.

After a crystal has been machined to produce a wafer with the desired characteristics, the wafer is bonded between contact discs. The resulting device can then be encapsulated in a variety of ways to meet differing environmental requirements, such as high rotational and vibrational forces.

Silicon carbide rectifiers have been operated for 1000 hours at temperatures up to 500 degrees C without appreciable degradation (Fig. 1). Some specially prepared units have been operated near 600 degrees C. Rectifiers having a peak forward current above 50 amperes have been tested and found to be stable.

Potential high-temperature applications include alternators and rectifier bridges for power conditioning. The devices are especially attractive for missiles and supersonic aircraft because they would require less cooling or none at all.

In addition to power rectifiers, silicon carbide diodes of milliampere current capacity have been made for various applications. For use in high-efficiency magnetic amplifiers, the diodes can be made with low reverse currents and matching forward characteristics. With suitable series connections, blocking diodes of up to 2000 peak reverse voltage have been prepared successfully.

The inherent radiation resistance should lead to other specialized applications (Fig. 2). One is use near nuclear reactors, as instrumentation diodes for example. Another is in power conditioning for vehicles operating in space.

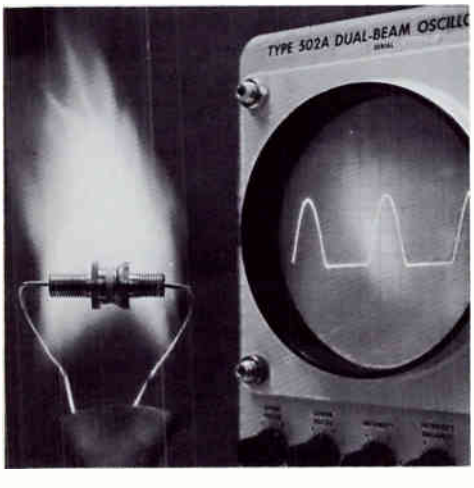

Although the encapsulated silicon carbide rectifier is exposed to a torch flame, its output is still a rectified signal.

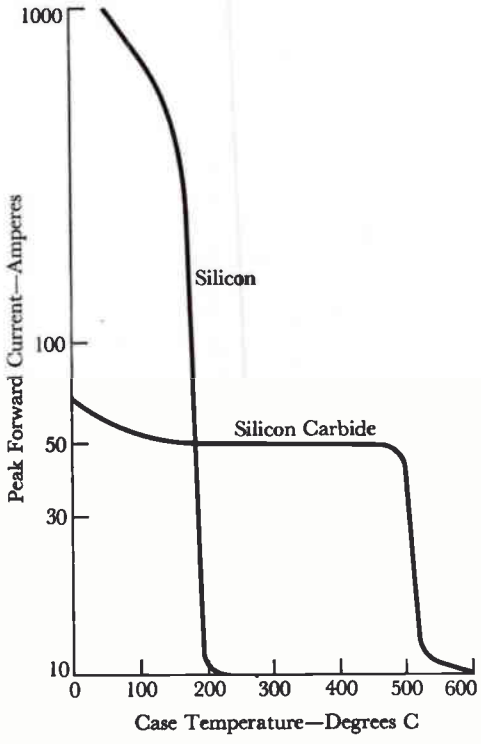

1—Silicon carbide rectifiers can operate at temperatures up to 500 degrees C with only slight current drop-off. Although silicon rectifiers can have much higher peak current ratings, they are restricted to use at temperatures below 200 degrees C. (Case temperature is the temperature of the outer package; the diode is at a higher temperature.)

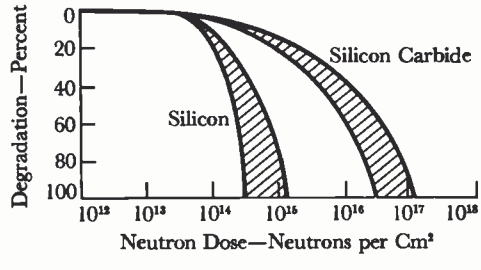

2—Silicon carbide rectifiers can be used in radiation doses up to 10^{16} neutrons per square centimeter without significant degradation and, in some specialized applications, up to 10^{17} neutrons per square centimeter. Comparable silicon rectifiers are nearly completely degraded at radiation doses above 10^{15} neutrons per square centimeter.

SEC Television Camera Tubes Map Ultraviolet Stars

Four 12-ounce television camera tubes are giving man a new look at his universe from their telescope mounts aboard the National Aeronautics and Space Administration's largest and most-instrumented unmanned satellite, the Orbiting Astronomical Observatory (OAO-A2). The Uvicon television camera tubes are mapping the stars and interstellar space in an experiment—called Project Celescope—conducted for NASA by the Smithsonian Astrophysical Observatory.

The mapping is done by means of far-ultraviolet radiation, which, though emitted by celestial bodies, never reaches the earth's surface because it is absorbed in the atmosphere. Thus, the orbiting Uvicons give pictures of the heavens that have previously been screened from earth-bound observation. Such pictures offer special promise for studying extremely hot young stars, some perhaps only 100,000 years old, whose major energy output is in the ultraviolet range. (Our own sun, which radiates mainly visible light and heat, is a relatively old cool star thought to be about five billion years old.) Study of the ultraviolet stars is expected to give new insight into their ages and chemical compositions and perhaps lead to new discoveries about how the universe came into being and is evolving.

Project Celescope dates back to the late 1950's, when the Smithsonian proposed it to NASA and began work with Westinghouse on development of the key Uvicon camera tube. The company's Electronic Tube Division and its Research Laboratories developed the tube jointly.

The project is scheduled to survey some 100,000 stars at a rate of up to 700 per day. An ultraviolet map of the entire sky will require about a year to complete.

The satellite has four high-resolution telescope systems. Each consists of three main components: an optical system (Schwarzschild telescope) to form the ultraviolet star images and focus them onto the camera tube; the tube, which amplifies the images electronically, stores them, and converts them into television-type electrical signals; and a digital television system that processes the signals for transmission back to earth, where the original ultraviolet pictures are reconstructed.

The Uvicon is an extremely sensitive camera tube. It is a member of a family of devices known as SEC image tubes (so called for "secondary electron conduction," the electronic amplification principle used). Ultraviolet images are focused on the input surface of the Uvicon through a window of a material such as lithium fluoride that does not absorb the wavelengths of interest. The back surface of the window is coated with a photosensitive material that releases electrons where the ultraviolet image strikes it. Those electrons are accelerated by high voltage toward the rear of the tube, where they strike a target that has a thin porous layer of potassium chloride.

The impact of each speeding electron on the target causes it to emit as many as 300 additional electrons, called secondary electrons, that are conducted through the porous layer to a metal film. There the electrons create an electric charge pattern that is an exact reproduction of the original ultraviolet image. The charge pattern is read out as electrical signals by scanning the target with a beam of electrons, and the signals then go to electronic circuitry that amplifies, codes, and stores them. On command from the ground, the coded information is transmitted to earth and fed to decoding circuitry that recreates the Uvicon's signals and, thereby, the ultraviolet pictures. The input windows and photosurfaces of the four Uvicons are designed to respond to four bands of ultraviolet radiation in the wavelength range from 1050 to 3000 angstroms. (For an application of SEC image tubes in earth-bound astronomy, see inside front cover.)

EMR, a division of Weston Instruments, Inc., is systems contractor for Project Celescope and was responsible for development of the ultraviolet telescopes and their associated electronic equipment. Grumman Aircraft Engineering Corporation is prime contractor for the OAO program.

Blast Furnace Automation Extended for High Production and Uniformity

The potential for cost reduction inherent in the basic oxygen steelmaking process depends on a process for making pig iron—the principal raw material—that is fast, efficient, and consistent. Consequently, steelmakers have been enlarging their blast furnace facilities, improving operating practices, and applying improved furnace control systems to obtain larger quantities of pig iron having more consistent and predictable quality.

Panels for a computer-automated blast furnace charging control system are checked before being shipped for installation.

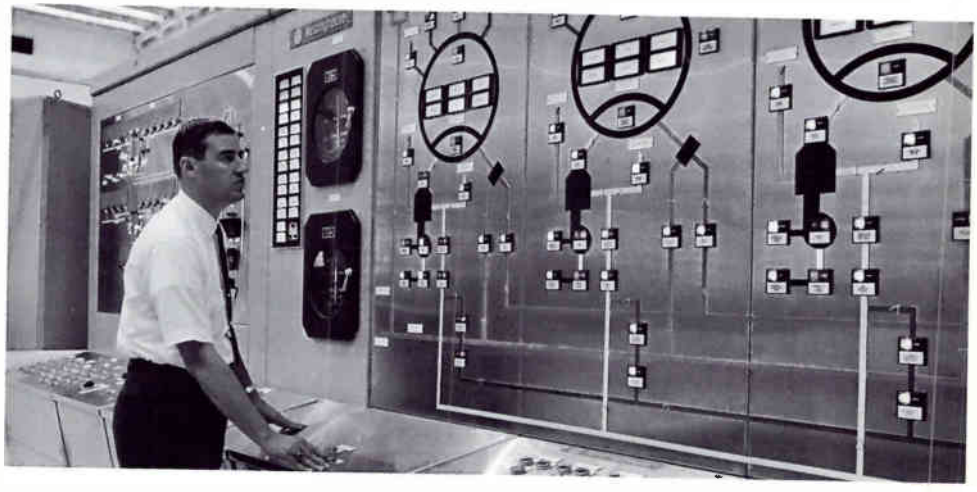

A computerized automatic furnace charging control system developed by the Westinghouse Industrial Systems Division is the latest step toward the goal of complete automation of the entire blast furnace complex with a closed-loop control system. It controls the weighing and sequencing of coke, limestone, iron ore, and other raw materials to assure efficient production of iron of the desired uniform composition. Use of the control system enables an average blast furnace to produce 4000 to 5000 tons a day.

Test Facility Begun for Breeder Reactor Development

Work has begun on the Fast Flux Test Facility, the major test location for fuels and materials in the U.S. Atomic Energy Commission's Liquid Metal Fast Breeder Reactor program. It is located near Richland, Washington, and is expected to be in operation in 1973.

The AEC is developing breeder reactors—nuclear reactors that produce more fissionable material than they consume—to conserve the available supplies of nuclear fuel materials. It will use the Fast Flux Test Facility for irradiation testing and post-irradiation examination of fuels and materials being considered for use in such reactors.

Westinghouse is providing reactor plant design services to Battelle-Northwest for the project. The company is responsible for design of the reactor and associated nuclear systems, with most of the work to be done by its Advanced Reactors Division. Atomics International Division of North American Rockwell is a subcontractor to Westinghouse.

Products for Industry

High-power tetrode cooled by forced air has been developed for oscillator, modulator, and amplifier applications in communications systems at frequencies up to 110 MHz. The compact ceramic and metal tetrode is designated WL-8171/4CX10,000. A pair of them can deliver 17.5 kW of audio-frequency or radio-frequency power with zero driving power. The tetrode has a plate dissipation rating of 10,000 W. It is approximately 9 inches long, has a maximum diameter of 5 inches, and weighs 9½ pounds. It is operated with its axis vertical and at temperatures below 250 degrees C. *Westinghouse Electronic Tube Division, P.O. Box 284, Elmira, New York 14902.*

Enclosed high-voltage capacitors (Type IDP) for increasing the efficiency of plant distribution systems can be installed indoors or outdoors. The capacitors are rated 15, 25, 50, 75, and 100 kVAc at 2400 and 4160 volts. They are dustproof and corrosion proof, with a protective exterior finish of zinc and outdoor enamel paint. *Westinghouse Distribution Apparatus Division, P.O. Box 341, Bloomington, Indiana 47402.*

Hydraulic-pump motors provide long life and high power for aircraft and ground support equipment. The line of direct-drive pump motors is made up of 400-Hz units with three basic sets of ratings: 7 hp at 4600 r/min, 10 poles; 8 hp at 5700 r/min, 8 poles; 13 hp at 5700 r/min, 8 poles. Many combinations of ratings can be made from the basic models. All motors are 6.33 inches in diameter and from 7.25 to 9.25 inches long. They weigh from 20.0 to 26.5 pounds. The motors are housed in a one-piece metal shroud and mounted on a rib-reinforced foot. *Westinghouse Aerospace Electrical Division, Utilization Systems Department, P.O. Box 989, Lima, Ohio 45802.*

Static voltage regulator and associated static excitation switchgear are connected directly into the fields of existing main exciters to replace electromechanical regulators. The type PRX regulator controls generator terminal voltage by supplying a buck-boost control signal above and below the base excitation signal. Its sensing circuit responds to average three-phase voltage and is insensitive to frequency. It controls excitation by governing the firing circuit to vary the output of the power amplifier. *Westinghouse Switchgear Division, 700 Braddock Avenue, East Pittsburgh, Pennsylvania 15112.*

Services for Industry

Load-flow and stability computer programs provide analytical tools to resolve voltage fluctuation difficulties in steel-producing arc furnaces. A load-flow study determines the optimum system parameters, i.e., the impedance of the capacitor and reactor and the kvar rating of the condenser. Economics and steady-state voltage fluctuations are the design criteria. With those parameters selected, a stability study is performed to observe transient behavior of the synchronous condenser and to verify that its angular swing does not aggravate voltage disturbances at a critical bus. Consideration is given to furnace loading and to faults that produce severest disturbances. *Westinghouse Advanced Systems Technology, East Pittsburgh, Pennsylvania 15112.*

About the Authors

C. J. Baldwin joined Westinghouse in 1952 after obtaining his BSEE and MSEE degrees from the University of Texas. He was awarded the B. G. Lamme scholarship in 1956 and obtained a professional EE Degree at MIT.

Baldwin has had a variety of assignments in the Power System Planning Department. He is presently manager of development, Advanced Systems Technology, where he is responsible for developing new digital computer applications for solving power systems problems, and for managing Westinghouse consulting services for utility and industrial customers.

Baldwin was chosen for Eta Kappa Nu's Outstanding Young Electrical Engineer Award for 1961. In 1967, the University of Texas designated him a Distinguished Engineering Graduate. A key factor in his selection was his work in the development of power system simulation techniques.

Robert C. Fear, Robert R. Madson, and **Joseph M. Urish** all contributed to development of the propulsion and maneuvering system for the DSRV, and they bring a variety of technical backgrounds to its description in this issue.

Fear is a Supervisory Engineer in the solid-state systems development section at the Aerospace Electrical Division, with the added responsibility for planning and coordination of in-house and contractual programs for development and production of deep submergence motors, controllers, and associated equipment. He joined Westinghouse on the graduate student training program in 1957 after graduating from Purdue University with a BSEE. Fear was assigned to the Aerospace Electrical Division, where he contributed to the development of oil-cooled aircraft generators, an electrostatic generator design and test program, generator design and systems studies for space power, and electrical design of submersible motors. He was made program manager for DSRV propulsion systems in 1967 and became Manager of Deep Submergence Programs in 1968. He assumed his present position last December.

Madson graduated from Illinois Institute of Technology with a BSME in 1947. He joined International Harvester Corporation, working as a project engineer in the design, test, and manufacture of power train components and rotary equipment for off-highway and construction equipment. Madson joined Westinghouse in the former Nutall Division in 1956 for similar engineering work on hydrodynamic power shaft transmission products. He went to the Aerospace Electrical Division in 1961, where his responsibilities have included design of electric-powered hydrostatic propulsion equipment for vehicles, mechanical components for nuclear space power systems and lunar vehicle propulsion systems, and the mechanical parts of deep-submergence propulsion systems (including pressure containers).

Urish earned his electrical engineering degree at Wayne State University in 1965 and then joined Westinghouse on the graduate student training program. His first assignment was with the Materials Handling Group. In 1965 he moved to the Aerospace Electrical Division, where he contributed to the development of a lunar core drill and more recently has been project engineer for the DSRV motor controllers.

James C. Wachob has been designing and applying dc motors since he joined DC Motor Engineering in 1958. His contributions include development and application of special motors for machine tools, refinement of permanent-magnet motor theory, and application of permanent-magnet motors to new uses. Wachob graduated from North Carolina State University with a BEE in 1958 and has since taken graduate work through the University of Buffalo extension program.

John C. Erlandson earned his BSEE degree at Tri-State College in Indiana in 1957, and he also has taken graduate work through the University of Buffalo extension program. He joined Westinghouse on the graduate student training program and was assigned to DC Motor Engineering. He served as a design engineer, and then an interest in computer application led him to his present responsibility for development of computerized design programs for dc motors.

G. S. Rambo is Manager, Metals and Process Systems, Hagan/Computer Systems Division. He is responsible for the design, manufacture, and installation of computerized process control systems for the metals and process industries. Before assuming that position, his responsibilities had included being projects manager for computer projects in the steel-mill application area, project director for the computer portion of a large hot strip mill, and developer of software for sequencing control of a plate mill at Taranto, Italy.

Rambo graduated from Virginia Polytechnic Institute with a BSEE in 1961, and he earned a master's degree in engineering administration at George Washington University in 1964. He worked two years on design and installation of solid state telegraphy switching apparatus at Bendix Radio Division before joining Westinghouse in 1963.

Vester S. Buxton graduated from the University of Southwestern Louisiana in 1957 with a BSME degree, and he has since taken graduate work in electrical engineering at the University of Pittsburgh. He joined Westinghouse on the graduate student training program and worked first in the former Industry Systems Department. He contributed to the application of process controls in the paper industry, including a ground-breaking application—the first successful process control computer in that industry (for a digester at Gulf States Paper Corporation).

Buxton moved to Hagan/Computer Systems Division in 1964, where he applied another industry first—the first computer for mill position regulators and automatic gauge control (for an Armco Steel Corporation hot rolling mill). He is now the division's Industrial Sales Manager.

Louis P. Goetz graduated from the University of Idaho with a BSEE in 1938 and joined Westinghouse as a test engineer in 1940. His first work with radar began in 1941 when he served as a communications officer in the U.S. Army Signal Corps. After a year as an observer with the British, he was assigned to the Evans Signal Laboratory to work with radar research and development projects. Goetz continues to serve in the Army Reserve today as a colonel in the Signal Corps, commanding a research and development detachment.

In 1946, Goetz moved to the oil industry, where he worked for several companies, principally in the design of instrumentation for that industry. Goetz returned to radar and Westinghouse in 1955 when he joined the Aerospace Division to work in pulse doppler radar systems design. He is presently a staff engineer, associated with the system mechanization section of the radar systems group.

The wrapping machine in use here adds speed and precision to the job of wrapping a current transformer coil with insulating tape. It was developed by engineers at the Westinghouse Distribution Transformer Division.